NASA CONTRACTOR REPORT

NASA CR-15
c.1

NASA CR-1547

THIN RADIATING SHOCK LAYER ABOUT A BLUNT BODY

by Y. S. Chou and L. H. Blake

Prepared by
LOCKHEED AIRCRAFT CORPORATION
Palo Alto, Calif.
for Ames Research Center

NATIONAL AERONAUTICS AND SPACE ADMINISTRATION • WASHINGTON, D. C. • MARCH 1970

THIN RADIATING SHOCK LAYER ABOUT A BLUNT BODY

By Y. S. Chou and L. H. Blake

Mar 70

Prepared under Contract No. NAS 7-632 by
LOCKHEED AIRCRAFT CORPORATION
Pala Alto, Calif.

for Ames Research Center

NATIONAL AERONAUTICS AND SPACE ADMINISTRATION

For sale by the Clearinghouse for Federal Scientific and Technical Information
Springfield, Virginia 22151 – CFSTI price $3.00

FOREWORD

This report is one of two volumes covering work performed for the National Aeronautics and Space Administration Headquarters, Office of Advanced Research and Technology, under the terms and specifications of Contract NAS 7-632, issued through NASA Resident Office, Jet Propulsion Laboratory, 4800 Oak Grove Drive, Pasadena, California. Technical Monitor of this contract was Mr. William Page, Hypersonic Free-Flight Branch, NASA Ames Research Center, Moffett Field, California.

The work was performed in the Aerospace Sciences Laboratory (R. Capiaux, Manager), of the Lockheed Palo Alto Research Laboratory.

ABSTRACT

A theoretical study is performed of the flow in a thin shock layer about axisymmetric blunt bodies by a Blasius type series expansion technique. Solutions were obtained for three terms in the series, and the validity of the resulting solutions is shown to numerically converge away from the stagnation point to a body angle near the sonic line ($\sim 45^{\circ}$). The primary objective of the investigation was to determine the coupling experienced between the radiative and viscous transport. Consequently, solutions were obtained for both the viscous and inviscid models at three extreme earth reentry flight conditions. A real gas model which is both emitting and absorbing radiant energy in a three-band continuum radiation model was considered. The differential approximation method is used to describe the radiative transport. A cold, non-blowing wall is assumed and the Prandtl number as well as the viscosity-density ratio are assumed constant.

The results indicate a weak coupling between viscosity and the radiative flux distribution. The influence of radiative transport upon the convective heating is shown to be significant; however, the effect of radiative transport upon the velocity field is small.

ACKNOWLEDGMENTS

The authors would like to express their sincere appreciation to K. H. Wilson of the Laboratory for his helpful discussions and suggestions during the course of the work described in this report. Particular thanks are extended to H. R. Kirch for her many contributions in IBM programming and suggestions on the numerical analysis.

NOMENCLATURE

$A_{i,1}, A_{i,1} \cdots$	coefficients in the series expansion for integrated intensity
B	blackbody radiation
B_b	body bluntness $(b/a)^2$ (see Fig. 1)
B_ν	Planck function
C	speed of light
$f_1, f_2 \cdots$	coefficients in the series expansion for tangential velocity
$G_1, G_2 \cdots$	coefficients in first order enthalpy and velocity solutions
$g_1, g_2 \cdots$	coefficients in the series expansion for total enthalpy
H	total enthalpy
h	specific enthalpy, Planck constant
I_ν	spectral radiation intensity
I_o	integrated intensity
$\tilde{K}$	$1 + Ky$
k	body curvature, Boltzman constant
M	Mach number
m	mass
N	mass density viscosity ratio $\rho_s \mu_s / \rho \mu$
N_N	number density of nitrogen atoms
p	pressure
Pr	Prandtl number
$Q_{i,1}, Q_{i,2}$	coefficients in the series expansion for radiative heat flux

$(q_x)_\nu, (q_y)_\nu$	spectral radiative heat flux in the direction of x and y, respectively
$\dot{q}$	normalized total heat flux
r	distance measured from axis of symmetry
R_b	body radius of curvature at stagnation point
R_s	shock radius of curvature at stagnation point
Re	Reynolds number $\rho_\infty U_\infty R_s/\mu_{s(o)}$
T	temperature
u	velocity component parallel to the body
v	velocity component perpendicular to the body
$v_1, v_2 \cdots$	coefficients in the series expansion of normal velocity
x	distance parallel to the body measured from stagnation line
y	distance normal to the body
α_ν	absorption coefficient
β	degree of dissociation
γ	specific heat ratio C_p/C_v
Δ	shock layer thickness
ϵ	stagnation point density ratio across shock
η	normalized stream function
θ_d	dissociation energy
θ_i	ionization energy
ν	frequency
ξ_N	quantum mechanical correction factor for absorption coefficient
ρ	density
τ	normalized skin friction
ψ	stream function
ω	parametric variable defined by Eq. (74)

Subscripts

s	quantities at shock
b	quantities at body
o	quantities at stagnation line
i	iterative solution
N	nitrogen
e	electron
∞	free stream conditions

CONTENTS

CONTENTS (Cont'd)

Section 1
INTRODUCTION

The ability to predict the convective and radiative heating experienced by a reentry body at and away from its stagnation point is necessary for mission planning and vehicle design. To date the stagnation point analysis has been of primary interest. At the stagnation point, all physical mechanisms of energy transport are represented, and it is anticipated that the stagnation point represents the location of maximum heating. Consequently, the momentum and energy fields of the stagnation point have been described in somewhat complete detail (Ref. 1).

In order to obtain the complete heat load distribution, however, the convective and radiative heating loads away from the stagnation point are essential. The complexity of including the detail of the transport mechanisms into the complete momentum and energy equations around a body results in solutions which becomes prohibitively time consuming even with present-day numerical techniques. This investigation was to develop a simplified analysis to study the coupling between the momentum and energy transport mechanisms in a thin-radiating shock layer (viscous and inviscid) away from the stagnation point.

A Blasius type series representation of the inviscid, adiabatic, hypersonic shock layer about a blunt body has been shown to be adequate to the sonic line (Ref. 2). In this study, the same technique is employed to study the radiating shock layer

for both inviscid and viscous cases. As a result of this study, it is expected that the distribution of radiative heating around the body can be determined both qualitatively and quantitatively, that the effect of radiation energy loss on the velocity field and the degree of coupling between the gas dynamics and the energy distribution (radiative and convective fluxes) can be determined, and that the effect of boundary layer on radiative heating to the body (if any) can also be determined. The underlying concept of the formulation for velocity field can be found in Part I of Ref. 3. The radiative transfer equation is replaced by the well known differential approximation, e. g. Vincenti and Kruger (Ref. 4), and simplification is made assuming a thin layer which is consistent with those made in the fluid mechanics. A three-band model is used for the continuum absorption coefficient. In each band analytic expressions are available (Hoshizaki and Wilson, Ref. 5) that give explicitly the frequency dependence of the absorption coefficients. Thus proper integration can be performed in each of the frequency ranges and mean quantities such as radiative heat flux can be found in terms of the local thermodynamics. No line or molecular band radiation is included in this study. The body wall is assumed to be highly cooled in comparison with the gas behind the shock. Perfect gas thermodynamics are not assumed. The equation of state is obtained by curve-fitting the data based on numerical evaluation for air of Néel and Lewis (Ref. 6).

The details of the formulation in this study are outlined in Part II of Ref. 3. In this earlier work, however, only two terms of the series had been formulated and they are represented by a group of universal functions which were independent of particular body shape. In this study, no universal

function will be evaluated since we will only be interested in a specific type of body. Three terms of the series have been formulated and solved. Many errors contained in the Part II of Ref. 3 have been corrected in this study. An inviscid solution as well as viscous solution will be presented.

Section 2

ANALYSIS

2.1 GOVERNING EQUATIONS

The fluid conservation equations (mass, momentum, energy) for axisymmetric bodies, written in a body oriented coordinate system (Fig. 1), are:

$$\frac{\partial \rho u r}{\partial x} + \frac{\partial \rho v r \tilde{k}}{\partial y} = 0 \tag{1}$$

$$\rho u \frac{\partial u}{\partial x} + \rho v \tilde{k} \frac{\partial u}{\partial y} = - \frac{\partial p}{\partial x} + \frac{\partial}{\partial y}\left(\mu \frac{\partial u}{\partial y}\right) - \rho k u v \tag{2}$$

$$\tilde{k} \frac{\partial p}{\partial y} = k u^2 \rho \tag{3}$$

$$\rho u \frac{\partial H}{\partial x} + \tilde{k} \rho v \frac{\partial H}{\partial y} = \frac{\partial}{\partial y}\left(\frac{\mu}{Pr} \frac{\partial H}{\partial y}\right) + \frac{\partial}{\partial y}\left[\frac{\mu\left(1 - \frac{1}{Pr}\right)}{2} \frac{\partial u^2}{\partial y}\right] + \int_0^\infty \alpha_\nu \left[\int_0^{4\pi} I_\nu d\Omega - 4\pi B_\nu\right] d\nu \tag{4}$$

The y-momentum equation has been simplified by retaining only the terms of order unity.

The radiation field is coupled with the fluid mechanics through the integral term in the energy Eq. (4) which represents the radiative energy loss or gain per unit volume.

In seeking solutions of the radiative transfer equation, we will use the differential approximation. In the present case of a thin hot gas with a cold

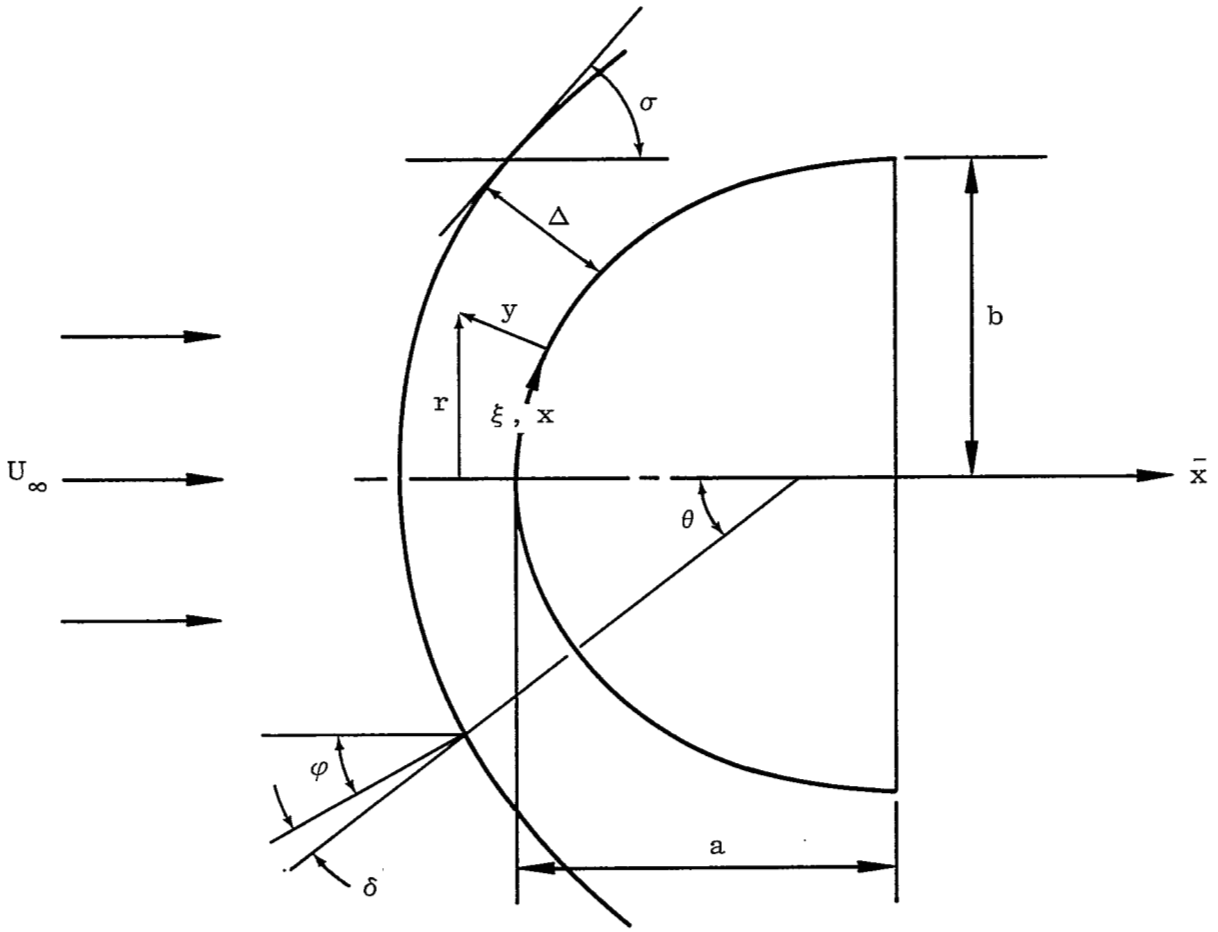

Fig. 1 Sketch of Geometry

wall and cool gas in front of the shock, the differential approximation has been suggested as a valid description of the radiative transport (i.e. Ref. 4). In the framework of the differential approximation, the radiative transfer equation is approximated by the following set of equations.

$$\nabla \cdot q_\nu = - \alpha_\nu [(I_o)_\nu - 4\pi B_\nu] \tag{5a}$$

with

$$\frac{\partial (I_o)_\nu}{\partial y} = - 3\alpha_\nu (q_y)_\nu \tag{6}$$

$$\frac{\partial (I_o)_\nu}{\partial x} = - 3\alpha_\nu (q_x)_\nu \tag{7}$$

In the case of the thin shock layer, $\partial/\partial x \ll \partial/\partial y$, and we make the approximation that*

$$\nabla \cdot q_\nu \simeq \frac{\partial (q_y)_\nu}{\partial y}$$

Thus, Eq. (5a) becomes

$$\frac{\partial (q_y)_\nu}{\partial y} = - \alpha_\nu [(I_o)_\nu - 4\pi B_\nu] \tag{5b}$$

One immediate consequence of this thin layer simplification is that Eqs. (5b) and (6) are sufficient for the determination of q_y and I_o; Eq. (7) is only needed for calculating q_x.

---

*The error introduced by this approximation is shown to be of the order ϵ^2 (Appendix II).

We will now consider only the absorption coefficient α_ν for continuum radiation and neglect the line and molecular band radiation. We will also take the three band model for α_ν; namely, we approximate α_ν by three analytic expressions in three different frequency ranges of the spectrum. The specific form of α_ν and the range of frequency interval will be presented in the next section. Here we will represent the frequency interval generally by $(\Delta h\nu)_i$, $i = 1,2,3$. We then define

$$(\alpha q_y)_i = \int_{(\Delta h\nu)_i} \alpha_\nu (q_y)_\nu \, d\nu \, , \quad (\alpha I_o)_i = \int_{(\Delta h\nu)_i} \alpha_\nu (I_o)_\nu \, d\nu \, , \quad B_i = \int_{(\Delta h\nu)_i} \alpha_\nu B_\nu d\nu \tag{8}$$

Clearly

$$\alpha q_y = \int_o^\infty \alpha_\nu (q_y)_\nu d\nu = \sum_i (\alpha q_y)_i$$

$$\alpha I_o = \int_o^\infty \alpha_\nu I_\nu d\nu = \sum_i (\alpha I_o)_i \tag{9}$$

$$B = \int_o^\infty \alpha_\nu B_\nu d\nu = \sum_i B_i$$

With substitution of Eqs. (9), Eq. (4) and the radiative transfer Eqs. (5b) and (6) (after integration with respect to frequency) then become

$$\rho u \frac{\partial H}{\partial x} + \tilde{k}\rho v \frac{\partial H}{\partial y} = \frac{\partial}{\partial y}\left(\frac{\mu}{Pr}\frac{\partial H}{\partial y}\right) + \frac{\partial}{\partial y}\left[\mu\left(1 - \frac{1}{Pr}\right)\frac{\partial}{\partial y}\left(\frac{u^2}{2}\right)\right] + \sum_{i=1}^{3}\left[(\alpha I_o)_i - 4\pi B_i\right] \tag{10}$$

$$\frac{\partial (q_y)_i}{\partial y} = - \left[(\alpha I_o)_i - 4\pi B_i \right] \tag{11}$$

$$\frac{\partial (I_o)_i}{\partial y} = - 3(\alpha q_y)_i \tag{12}$$

We now proceed to normalize the variables. The distances x, y and the distance from the axis, r, are normalized by the stagnation point shock radius R_s, the velocities u, v by the free stream velocity u_∞, the density ρ by the free stream density ρ_∞, the pressure p by twice the free stream kinetic pressure $\rho_\infty u_\infty^2$, the body (or shock) curvature k by $1/R_s$, the total enthalpy H as well as the static enthalpy h by H_s and, finally, the stream function ψ by $\rho_\infty u_\infty R_s^2$. The temperature is normalized by the temperature immediately behind the normal shock $T_{s(o)}$, the viscosity by its value immediately behind the normal shock $\mu_{s(o)}$ and q, I_o, B are all normalized by the quantity $[kT_{s(o)}]^4/h^3c^2$. From here on, the equations are all written in nondimensional form.

$$\xi(x) = \epsilon \int_o^x \rho_s \mu_s dx \ , \quad \eta(x,y) = \frac{\psi}{r_s^2} \ , \quad d\psi = \rho u r \, dy - \rho v r \tilde{k} \, dx \tag{13}$$

the conservation equations can then be written in ξ, η coordinates as

$$\rho u \left(r_2^2 \frac{\partial u}{\partial \xi} - \eta \frac{dr_s^2}{d\xi} \frac{\partial H}{\partial \eta} \right) = - \left(r_s^2 \frac{\partial p}{\partial \xi} - \eta \frac{dr_s^2}{d\xi} \frac{\partial p}{\partial \eta} \right) + \frac{N}{\epsilon Re} \rho u \frac{\partial}{\partial \eta} \left(u \frac{\partial u}{\partial \eta} \right) \tag{14}$$

$$\frac{\partial p}{\partial \eta} = k u r_s \tag{15}$$

$$\epsilon\rho_s\mu_s u\left[r_s^2\frac{\partial H}{\partial\xi} - \eta\frac{dr_s^2}{d\xi}\frac{\partial H}{\partial\eta} - \frac{N}{\epsilon RePr}\left(u\frac{\partial H}{\partial\eta}\right) - \frac{N}{\epsilon Re}\left(1-\frac{1}{Pr}\right)\frac{\partial}{\partial\eta}\left(u^2\frac{\partial u}{\partial\eta}\right)\right] = r_s^2\sum_i \Gamma_i[(\alpha I_o)_i - 4\pi B_i] \tag{16}$$

$$u\frac{\partial(q_\eta)_i}{\partial\eta} = -\lambda_i r_s[(\alpha I_o)_i - 4\pi B_i] \tag{17}$$

$$u\frac{\partial(I_o)_i}{\partial\eta} = -3\lambda_i r_s(\alpha q_\eta)_i \tag{18}$$

with $i = 1,2,3$ and $Re = \rho_\infty U_\infty R_s/\mu_{s(o)}$.

In Eqs. (14) and (16) the following approximation and assumption were made; namely, $r \simeq r_s$ and $\rho\mu/\rho_s\mu_s = N$ = constant.

Expressions for the radiation parameters λ_i and Γ_i will be given in the next section after α_ν is specified.

Equations (14) and (18) are to be solved by satisfying the proper boundary conditions and a state equation (given in the next section). The boundary conditions for the flow field are given as follows:

at the shock,

$\eta = 1/2$,

$u = u_s$, $p = p_s$, $\rho = \rho_s$, $H = H_s$

and H_s, u_s, p_s, ρ_s are given by oblique shock relations;

at the body,

$\eta = 0$,

$u = 0$,

$H = g_b$.

For the radiation field, the differential approximation gives us the condition: at the shock,

for cold gas ahead of the shock, we have $I_o - 2q_y = 0$, which then implies $(I_o)_i - 2(q_y)_i = 0$ for all i.

at the body,

the cold wall assumption $I_o + 2q_y = 0$. Thus, $(I_o)_i + 2(q_y)_i = 0$, for all i.

2.2 GAS PROPERTIES

Curve fitting of the equilibrium properties of air calculated in Ref. 6 suggests the following approximate equation of state:

$$p = 10^{-2.5}\, \rho \left(\frac{h}{R}\right)^{0.84} \tag{19a}$$

with p in atm., ρ is amagat, and h/R in degree Kelvin. This then implies that in the normalized form, the equation of state is

$$\frac{p}{p_s} = \frac{\rho}{\rho_s} \left(\frac{h}{h_s}\right)^{0.84} \tag{19b}$$

Another equation of state for air is also available, namely

$$\rho = 1.65 \times 10^{-5}\, p(T/10^4)^{-1.72} \ \frac{gm}{cm^3} \tag{20}$$

where p is in atms and T is in ^oK. Equations (19) and (20) thus completely specify the equilibrium thermodynamic properties in air.

In the hypersonic limit, i.e., $h_\infty \ll 1/2\ U_\infty^2 (H_\infty = H_s \simeq 1/2\ U_\infty^2)$, the thermodynamic properties immediately behind the shock at the stagnation point are completely determined by ρ_∞ and U_∞. This is shown as follows: From Eq. (20), after normalizing T by $T_{s(o)}$, p by $\rho_\infty U_\infty^2$, ρ by ρ_∞, one can write

$$T = C_1 \left(\frac{p}{\epsilon\rho}\right)^{\frac{1}{1.72}} \tag{21a}$$

with

$$C_1 = \frac{10^4}{T_{s(o)}} \left(\frac{1.65\ \epsilon U_\infty^2}{10^{11}}\right)^{\frac{1}{1.72}} \tag{21b}$$

We note all quantities in Eq. (21b) should be in c.g.s. ^oK units. Now since at the stagnation point $T = 1$, $p = 1 - \epsilon$ and $\rho = 1/\epsilon$, Eq. (21a) immediately yields a relation

$$C_1 = \left(1-\epsilon\right)^{-\frac{1}{1.72}} \simeq 1 \text{ (for } \epsilon \ll 1) \tag{22}$$

Applying Eq. (19a) at the stagnation point behind the shock, we have the relation for hypersonic flow [i.e., $h_{s(o)} \approx \frac{1}{2} U_\infty^2$]

$$\epsilon(1-\epsilon) = \frac{10^{6.5}}{1.29\ U_\infty^2} \left(\frac{U_\infty^2}{2R}\right)^{0.84} \tag{23}$$

in Eq. (23). R is the universal gas constant and the unit of U_∞^2/R should always be in ^oK.

Equations (21b) and (23) thus give two relations to determine ϵ and $T_{s(o)}$ for a given ρ_∞ and U_∞.

From these considerations, we conclude that in the hypersonic limit, the independent parameters in our problem are the flight condition (ρ_∞, U_∞), Prandtl number, viscosity-density product ratio, and characteristic length R_s. The parameter R_s is an independent parameter since it appears in the radiative transfer parameters explicitly.

The analytic expression for the absorption coefficient in our three band model is taken from Hoshizaki and Wilson (Ref. 5). In fact, in Ref. 5 the expressions are given for more than three bands, for accuracy. However, we group them into only three. In addition, the contributions from ions are neglected and we treat oxygen as if it were nitrogen. In other words, in the calculation of absorption coefficients, we model air by a pure nitrogen gas. In this model, we write

$$\alpha_\nu = (1 - e^{-h\nu/kT})(K_\nu)_N \tag{24a}$$

with

$$(K_\nu)_N = 4.5\,\tilde{a}\,N_N kT e^{-(14.3-h\nu)/kT}\,\frac{\xi_N}{(h\nu)^3} \qquad 0 \le h\nu \le 4.22 \tag{24b}$$

$$(K_\nu)_N = 4.5\,\tilde{a}\,N_N kT\,\frac{\xi_N}{(h\nu)^3}\,e^{-10.08/kT} \qquad 4.22 \le h\nu \le 10.8 \tag{24b}$$

$$(K_\nu)_N = N_N \cdot \varphi_{N,1} \qquad 10.8 < h\nu \le 12.0 \tag{24c}$$

$$(K_\nu)_N = N_N(\varphi_{N,1} + \varphi_{N,2}) \qquad 12.0 < h\nu \le \infty \tag{24d}$$

and

$$\varphi_{N,1} = 5.16 \times 10^{-17}\, e^{-3.5/kT}/(4 + 10\, e^{-2.38/kT} + 6\, e^{-3.57/kT})$$

$$\varphi_{N,2} = 6.4 \times 10^{-17}\, e^{-2.3/kT}/(4 + 10\, e^{-2.38/kT} + 6\, e^{-3.57/kT}) \qquad (24e)$$

$$\tilde{a} = 7.28 \times 10^{-16}\ cm^2 - eV^2$$

where N_N is the number density of nitrogen atoms and ξ_N is the quantum mechanical correction factor. We approximate ξ_N by

$$\xi_N = 0.24 + 0.0426\,(h\nu - 4.22)^2 \qquad (25)$$

The ranges of the three-band model are chosen as $(\Delta h\nu)_1$, $0 \le h\nu \le 10.8$, $(\Delta h\nu)_2$, $10.8 \le h\nu \le 12$, $(\Delta h\nu)_3$, $12 \le h\nu \le \infty$.

In the first band $(\Delta h\nu)_1$, α_ν is small, and the optical depth (in this range of frequency and based on the shock layer thickness) is much less than unity. Hence it is reasonable to approximate α_ν in this range by its partial Planck mean, defined as

$$\alpha_1' = \frac{\int_{(\Delta h\nu)_1} \alpha_\nu B_\nu d\nu}{\int_{(\Delta h\nu)_1} B_\nu d\nu} \qquad (26)$$

The superscript (') denotes dimensional quantities.

In the second and third bands, $h\nu/kT$ is large, consequently $e^{-h\nu/kT} \ll 1$. And we can take α_2', α_3' as independent of frequency, i.e.,

$$\alpha_2' = N_N \varphi_{N,1} \tag{26a}$$

$$\alpha_3' = N_N(\varphi_{N,1} + \varphi_{N,2}) \tag{26b}$$

By using Eqs. (26), (26a) and (26b), one finds

$$\begin{aligned}(\alpha' q_y')_i &= \alpha_i'(q_y')_i \\ (\alpha' I_o)_i &= \alpha_i'(I_o)_i\end{aligned} \tag{27}$$

and after performing the integration, α_1', B_1', B_2', B_3' are found to be (kT is of order 1)

$$\alpha_1' = \frac{9\,\tilde{a}\,N_N\, e^{-14.3/kT}\{2.1 + kT[0.24 + 0.0853(kT)^2]\}}{(kT)^3\left\{\frac{2\pi^4}{15} - 2\,e^{-10.8/kT}\left[\left(\frac{10.8}{kT}\right)^3 + 3\left(\frac{10.8}{kT}\right)^2 + 6\left(\frac{10.8}{kT}\right) + 6\right]\right\}} \tag{28}$$

$$B_1' = \frac{9\,\tilde{a}\,N_N kT}{h^3c^2}\, e^{-14.3/kT}\,\{2.1 + kT[0.24 + 0.0853(kT)^2]\} \tag{29}$$

$$B_2' = \frac{2N_N\varphi_{N,1}}{h^3c^2}\,(kT)^4\left\{e^{-10.8/kT}\left[\left(\frac{10.8}{kT}\right)^3 + 3\left(\frac{10.8}{kT}\right)^2 + 6\left(\frac{10.8}{kT}\right) + 6\right]\right.$$

$$\left. - e^{-12/kT}\left[\left(\frac{12}{kT}\right)^2 + 3\left(\frac{12}{kT}\right)^2 + 6\left(\frac{12}{kT}\right) + 6\right]\right\} \tag{30}$$

$$B_3' = \frac{2N_N(\varphi_{N,1} + \varphi_{N,2})}{h^3c^3}\,(kT)^4\, e^{-12/kT}\left[\left(\frac{12}{kT}\right)^3 + 3\left(\frac{12}{kT}\right)^2 + 6\left(\frac{12}{kT}\right) + 6\right] \tag{31}$$

The atom number density N_N is related to the total number density (and eventually density) by taking the following model. Namely, we assume that there will be no ionization before the gas is totally dissociated. In the dissociation phase, we relate the atom number density to the total number density by using the Lighthill's ideal dissociation model. For the ionization phase, we assume the gas is in Saha equilibrium. Hence, for the dissociation phase, we have

$$N_N = \beta N_t \tag{32a}$$

$$\frac{\beta^2}{1 - \beta^2} = \frac{\rho_d R_{A_2} T e^{-\theta d/T}}{P} , \tag{32b}$$

$$R_{A_2} = \frac{K}{2m}$$

and for the ionization phase

$$N_N = (1 - \varphi) N_t \tag{33a}$$

$$\frac{\varphi^2}{1 - \varphi^2} = C \frac{T^{5/2}}{p} e^{-\theta_i/T} \tag{33b}$$

$$C = 2 \left(\frac{2\pi m_e}{h^2}\right)^{3/2} k^{5/2} \tag{33c}$$

By using the relations (26) to (33), one can find the expressions (in non-dimensional form) for α's, B's, λ's and Γ's involved in the energy Eq. (16) and the radiative transfer Eqs. (17) and (18) are as follows:

$$\alpha_1 = \begin{pmatrix} \beta \\ 1 - \varphi \end{pmatrix} \frac{T^{-3}\, e^{-C_4/T}[2.1 + C_5 T + C_6 T^3]}{\frac{2\pi^4}{15} - 2\, e^{-a/T}\left[\left(\frac{a}{T}\right)^3 + 3\left(\frac{a}{T}\right)^2 + \frac{6a}{T} + 6\right]} \tag{34}$$

$$\alpha_2 = \begin{pmatrix} \beta \\ 1 - \varphi \end{pmatrix} e^{-C_7/T}/(4 + 10\, e^{-C_8/T} + 6\, e^{-C_7/T}) \tag{35}$$

$$\alpha_3 = \begin{pmatrix} \beta \\ 1 - \varphi \end{pmatrix} e^{-C_7/T}(1 + 1.24\, e^{C_9/T})/(4 + 10\, e^{-C_8/T} + 6\, e^{-C_7/T}) \tag{36}$$

$$B_1 = \begin{pmatrix} \beta \\ 1 - \varphi \end{pmatrix} T\, e^{-C_4/T}(2.1 + C_5 T + C_6 T^3) \tag{37}$$

$$B_2 = 2T\left\{e^{-a/T}(a^3 + 3a^2T + 6aT^2 + 6T^3) - e^{-b/T}\left[(b^3 + 3b^2T + 6bT^2 + 6T^3)\right]\right\} \tag{38}$$

$$B_3 = 2T\, e^{-b/T}(b^3 + 3b^2T + 6bT^2 + 6T^3) \tag{39}$$

$$\lambda_1 = \frac{9\,\tilde{a}\, R_s \rho_\infty}{m[kT_{s(o)}]^3} \quad , \quad \lambda_2 = \lambda_3 = \frac{5.16 \times 10^{-17}\, \rho_\infty R_s}{m} \tag{40}$$

$$\Gamma_1 = \Gamma\lambda_1 \quad , \quad \Gamma = \frac{2[kT_{s(o)}]^4}{h^3 c^2 \rho_\infty U_\infty^3} \quad , \quad \Gamma_2/\Gamma_1 = \lambda_2/\lambda_1 \tag{41}$$

with

$$a = \frac{10.8}{kT_{s(o)}} \ , \ b = \frac{12}{kT_{s(o)}} \ , \ C_4 = \frac{14.3}{kT_{s(o)}} \ , \ C_5 = 0.24 \ kT_{s(o)} \ ,$$

$$\theta_d = \frac{9.7}{kT_{s(o)}} \ , \ \theta_i = \frac{14.53}{kT_{s(o)}} \ , \ C_6 = 0.058 \ [kT_{s(o)}]^2 \ , \ C_7 = \frac{3.5}{kT_{s(o)}} \ ,$$

$$C_8 = \frac{2.38}{kT_{s(o)}} \ , \ C_9 = \frac{1.2}{kT_{s(o)}} \qquad (43)$$

where $kT_{s(o)}$ in eV.

The factor $(1 - \beta\varphi)$ in front of Eqs. (34) to (37) denotes that during the dissociation phase, the value β should be used and during the ionization phase $(1 - \varphi)$ should be used

2.3 SERIES FORMULATION

Similar to Part I of reference 3, one can write the following series expression immediately behind the shock (See Appendix IV):

$$\begin{aligned}
u_s &= \xi + u_1\xi^3 + u_2\xi^5 + \ldots \\
r_s &= \xi + r_1\xi^3 + r_2\xi^5 + \ldots \\
p_s &= 1 - \xi^2 + p_2\xi^4 + \ldots \\
\rho_s &= \frac{1}{\epsilon}\left(1 - \rho_1\xi^2 - \rho_2\xi^4 + \ldots\right) \\
k_s &= 1 + k_1\xi^2 + k_2\xi^4 + \ldots \\
\mu_s &= 1 - \mu_1\xi^2 - \mu_2\xi^4 + \ldots
\end{aligned} \qquad (44)$$

These expressions are valid under the approximation of the thin layer concept, i.e., we have approximated the factor u_o, which should appear as a factor in the expressions of u_s and r_s, by taking $u_o = (d\xi_s/d\xi)_o = 1$. This approximation is reasonable for small values of ϵ. We also note that in the expression for p_s, we have neglected the term ϵ, by setting $1 - \epsilon \simeq 1$.

Based on Eq. (44), we assume the dependent variables can be written as

$$
\begin{aligned}
u &= f_1(\eta)\xi + u_1 f_2(\eta)\xi^3 + u_2 f_3(\eta)\xi^5 + \ldots \\
H &= g_1(\eta) + g_2(\eta)\xi^2 + g_3(\eta)\xi^4 + \ldots \\
(I_o)_i &= A_{i,1}(\eta) + A_{i,2}(\eta)\xi^2 + A_{i,3}(\eta)\xi^4 + \ldots \\
(q_y)_i &= Q_{i,1}(\eta) + Q_{i,2}(\eta)\xi^2 + Q_{i,3}(\eta)\xi^4 + \ldots
\end{aligned}
\tag{45}
$$

Also, from the discussion in the previous section, we can write

$$T = T_1(1 + T_2\xi^2 + T_3\xi^4 + \ldots) \tag{46}$$

$$\beta = \beta_1(1 + \beta_2\xi^2 + \beta_3\xi^4 + \ldots) \tag{47}$$

$$\varphi = \varphi_1(1 + \varphi_2\xi^2 + \varphi_3\xi^4 + \ldots) \tag{48}$$

After using an approximate series representation for the exponential function (see Appendix III), we obtain

$$B_i = B_{i,0}(B_{i,1} + B_{i,2}\xi^2 + B_{i,3}\xi^4 + \ldots) \tag{49}$$

$$\alpha_i = \alpha_{i,0}(\alpha_{i,1} + \alpha_{i,2}\xi^2 + \alpha_{i,3}\xi^4 + \ldots) \tag{50}$$

$i = 1,2,3.$

All coefficients are defined in Appendix I.

Substituting Eqs. (44) to (50) into the governing Eqs. (14) to (18) and collecting the same power of ξ, we obtain the equations for f_1, g_1, $A_{i,1}$, $Q_{i,1}$, f_2, g_2, $A_{i,2}$, $Q_{i,2}$, f_3, g_3, $A_{i,3}$ and $Q_{i,3}$ (we note the pressure is obtained by integrating Eq. (15)).

FIRST ORDER

$$f_1\left(f_1 - 2\eta \frac{df_1}{d\eta}\right) = 3\epsilon g_1^{0.84} + \frac{N}{\epsilon Re} f_1 \frac{d}{d\eta}\left(f_1 \frac{df_1}{d\eta}\right) \tag{51}$$

$$2\eta f_1 \frac{dg_1}{d\eta} + \frac{N}{\epsilon RePr} f_1 \frac{d}{d\eta}\left(f_1 \frac{dg_1}{d\eta}\right) + F_1(g_1) = 0 \tag{52}$$

$$f_1 \frac{dQ_{1,1}}{d\eta} = -\lambda_1 \alpha_{1,1}(\alpha_{1,0} A_{1,1} - 4\pi B_{1,0}) \tag{53}$$

$$f_1 \frac{dQ_{i,1}}{d\eta} = -\lambda_i \alpha_{o,0} \alpha_{i,1}(A_{i,1} - 4\pi B_{i,1}) \qquad i = 2,3 \tag{54}$$

$$f_1 \frac{dA_{i,1}}{d\eta} = -3\lambda_i \alpha_{i,0} \alpha_{i,1} Q_{i,1} \qquad i = 1,2,3 \tag{55}$$

SECOND ORDER

$$\frac{N}{\epsilon Re} f_1 \frac{d}{d\eta}\left(f_2 \frac{df_1}{d\eta} + f_1 \frac{df_2}{d\eta}\right) - f_1\left(3f_2 - 2\eta \frac{df_2}{d\eta}\right) - \frac{3\epsilon f_2 g_1^{0.84}}{f_1}$$

$$+ \frac{2.52}{u_1} \epsilon g_1^{-0.16} g_2 - 2\frac{r_1}{u_1} f_1\left(f_1 - 4\eta \frac{df_1}{d\eta}\right) + \frac{\epsilon g_1^{0.84}}{u_1}\left[3\left(\frac{1}{2} - \eta\right) + 2.52\left(1 - \frac{f_1^2}{g_1}\right) + H_1 + 3\rho_1 = 0\right. \tag{56}$$

$$f_1 \left\{ \frac{N}{\epsilon RePr} \left[\frac{d}{d\eta} \left(f_1 \frac{dg_2}{d\eta} \right) + u_1 \frac{d}{d\eta} \left(f_2 \frac{dg_1}{d\eta} \right) \right] + 2\eta \frac{dg_2}{d\eta} \right\} - \left(\frac{u_1 f_2}{f_1} - \mu_1 \right.$$

$$\left. - 2r_1 \right) F_1 - 2g_2 f_1 + 8r_1 \eta f_1 \frac{dg_1}{d\eta} + \frac{N}{\epsilon RePr} \left(1 - \frac{1}{Pr} \right) f_1 \frac{d}{d\eta} \left(f_1^2 \frac{df_1}{d\eta} \right)$$

$$+ F_2 = 0 \tag{57}$$

$$f_1 \frac{dQ_{1,2}}{d\eta} + u_1 f_2 \frac{dQ_{1,1}}{d\eta} = - \lambda_1 \left[r_1 (\alpha_{1,0} \alpha_{1,1} A_{1,i} - 4\pi B_{1,0} B_{1,1}) \right.$$

$$\left. + \alpha_{1,0} \alpha_{1,2} A_{1,1} + \alpha_{1,0} \alpha_{1,1} A_{1,2} - 4\pi B_{1,0} B_{1,2} \right] \tag{58}$$

$$f_1 \frac{dQ_{i,2}}{d\eta} + u_1 f_2 \frac{dQ_{i,1}}{d\eta} = - \lambda_i \left[\alpha_{i,0} (A_{i,1} - 4\pi B_{i,1}) (r_1 \alpha_{i,1} + \alpha_{i,2}) \right.$$

$$\left. + \alpha_{i,0} \alpha_{i,1} (A_{i,2} - 4\pi B_{i,2}) \right] \qquad i = 2,3 \tag{59}$$

$$f_1 \frac{dA_{i,2}}{d\eta} + u_1 f_2 \frac{dA_{i,1}}{d\eta} = - 3\lambda_i \left[r_1 \alpha_{i,0} \alpha_{i,1} Q_{i,1} + \alpha_{i,0} \alpha_{i,2} Q_{i,1} \right.$$

$$\left. + \alpha_{i,0} \alpha_{i,1} Q_{i,2} \right] \qquad i = 1,2,3 \tag{60}$$

THIRD ORDER

$$\frac{N}{\epsilon Re} f_1 \left\{ \frac{d^2(f_1 f_3)}{d\eta^2} + \frac{2u_1^2 f_2}{u_2 f_1} \frac{d^2(f_1 f_2)}{d\eta^2} + \frac{u_1^2}{u_2} \left[\left(\frac{df_2}{d\eta} \right)^2 + \left(\frac{f_2}{f_1} \right)^2 \left(\frac{df_1}{d\eta} \right)^2 \right.\right.$$

$$\left.\left. - \frac{2f_2}{f_1} \frac{df_1}{d\eta} \left(\frac{df_2}{d\eta} \right) \right] \right\} - \frac{3\epsilon f_3}{f_1} g_1^{0.84} - \frac{u_1^2}{u_2} \frac{f_2^2}{f_1^2} \left(f_1^2 - 2\eta f_1 \frac{df_1}{d\eta} - 3\epsilon g_1^{0.84} \right)$$

$$- \frac{f_1}{u_2} \left[(2r_2 + r_1^2) f_1 + 5u_2 f_3 + 6r_1 u_1 f_2 - 2\eta \, 3(2r_2 + r_1^2) \frac{df_1}{d\eta} + u_2 \frac{df_3}{d\eta} \right.$$

$$+ 4r_1u_1 \frac{df_2}{d\eta}\Big] - \frac{u_1f_2}{u_2}\left(2r_1f_1 + 3u_1f_2 - 2\eta\,(4r_1 \frac{df_1}{d\eta} + u_1 \frac{df_2}{d\eta})\right)$$

$$+ \frac{\epsilon g_1^{0.84}}{u_2}\,(3\sigma_2 + \sigma_1 H_1 + H_2) = 0 \qquad (61)$$

$$f_1\left\{\frac{N}{\epsilon RePr}\left[\frac{d}{d\eta}\,(u_2f_3 \frac{dg_1}{d\eta} + u_1f_2 \frac{dg_2}{d\eta} + f_1 \frac{dg_3}{d\eta})\right] + 2\eta\,\left(\frac{dg_3}{d\eta} + 4r_1 \frac{dg_2}{d\eta}\right.\right.$$

$$\left.\left. + 3 \frac{dg_1}{d\eta}\,(2r_2 + r_1^2)\right) - 4(r_1g_2 + g_3) + 2 \frac{N}{\epsilon Re}\,(1 - \frac{1}{Pr})\,u_1 \frac{d}{d\eta}\,(f_1f_2 \frac{df_1}{d\eta}\right.$$

$$\left. + \frac{f_1^2}{2} \frac{df_2}{d\eta})\right\} + F_1\left[(\frac{u_1f_2 - \mu_1f_1}{f_1})^2 - 2r_1\,(\frac{u_1f_2 - \mu_1}{f_1}) - \frac{u_2f_3 - \mu_1u_1f_2 - \mu_2f_1}{f_1}\right.$$

$$\left. + 2r_2 + r_1^2\right] + (2r_1 - \frac{u_1f_2 - \mu_1f_1}{f_1})\,F_2 + F_3 = 0 \qquad (62)$$

$$f_1 \frac{dQ_{1,3}}{d\eta} - (r_1f_1 - u_1f_2) \frac{dQ_{1,2}}{d\eta} - (r_2f_1 - u_2f_3 + u_1r_1f_2 - r_1^2f_1) \frac{dQ_{1,1}}{d\eta}$$

$$= - \lambda_1\left[\alpha_{1,0}\alpha_{1,1}A_{1,1} + \alpha_{1,0}\alpha_{1,2}A_{1,2} + \alpha_{1,0}\alpha_{1,3}A_{1,1} - 4\pi B_{1,0}B_{1,3}\right] \qquad (63)$$

$$f_1 \frac{dQ_{i,3}}{d\eta} - (r_1f_1 - u_2f_2) \frac{dQ_{i,2}}{d\eta} - (r_2f_1 - u_2f_3 + u_1r_1f_2 - r_1^2f_1) \frac{dQ_{i,1}}{d\eta}$$

$$= - \lambda_i\left[\alpha_{i,0}\alpha_{i,1}(A_{i,3} - 4\pi B_{i,3}) + \alpha_{i,0}\alpha_{i,3}(A_{i,2} - 4\pi B_{i,2})\right.$$

$$\left. + \alpha_{i,0}\alpha_{i,3}(A_{i,1} - 4\pi B_{i,1})\right] \qquad i = 2,3 \qquad (64)$$

$$f_1 \frac{dA_{i,3}}{d\eta} - (r_1 f_1 - u_1 f_2) \frac{dA_{i,2}}{d\eta} - (r_2 f_1 - u_2 f_3 + r_1 u_1 f_2 - r_1^2 f_1) \frac{dA_{i,1}}{d\eta}$$

$$= - 3\lambda_i \alpha_{i,0} \left[\alpha_{i,1} Q_{i,3} + \alpha_{i,2} Q_{i,2} + \alpha_{i,3} Q_{i,1} \right] \quad i = 1,2,3 \qquad (65)$$

See Appendix I for definitions of F_1, F_2, F_3, H_1, H_2, σ_1, σ_2. The boundary conditions for these equations are:

at wall $\quad f_1 = f_2 = f_3 = 0, \quad g_1 = g_b \quad g_2 = g_3 = 0$ *

$$A_{i,j} + 2Q_{i,j} = 0 \quad i = 1,2,3 \quad j = 1,2,3 \qquad (66)$$

at shock $\quad f_1 = f_2 = f_3 = 1 \quad g_1 = 1 \quad g_2 = g_3 = 0$

$$A_{i,j} - 2Q_{i,j} = 0 \quad i = 1,2,3 \quad j = 1,2,3$$

Since the ratio N/Re is zero for an assumed fluid model of zero viscosity, the energy and momentum equations for the inviscid case can be written from Eqs. (51), (52), (56), (57), (61), and (62).

FIRST ORDER

$$2\eta f_1 \frac{df_1}{d\eta} - f_1^2 + 3\epsilon g_1^{0.84} = 0 \qquad (67)$$

$$2\eta f_1 \frac{dg_1}{d\eta} + F_1 = 0 \qquad (68)$$

SECOND ORDER

$$2\eta f_1 \frac{df_2}{d\eta} - 3\left(f_1 + \frac{\epsilon g_1^{0.84}}{f_1}\right) f_2 + \frac{2.52\ \epsilon g_2}{u_1 g_1^{.16}}$$

$$+ \frac{2r_1 f_1^2}{u_1} + \frac{\epsilon g_1^{0.84}}{u_1} \left[3\left(\frac{1}{2} - \eta\right) + 2.52 \left(1 - \frac{f_1^2}{g_1}\right) + H_1 + 3\rho_1 - 12r_1 \right] = 0 \qquad (69)$$

* The wall is at constant temperature and is non-radiating.

$$2\eta f_1 \frac{dg_2}{d\eta} - 2f_1 g_2 - \left(\frac{u_1 f_2}{f_1} + 2r_1\right) F_1 + F_2 = 0 \qquad (70)$$

THIRD ORDER

$$2\eta f_1 \frac{df_3}{d\eta} - \left(5f_1 + \frac{3\epsilon g_1^{0.84}}{f_1}\right) f_3 + \frac{\epsilon g_1^{0.84}}{u_2} (3\sigma_2 + \sigma_1 H_1 + H_2) - \frac{\sigma_3}{u_2} = 0 \qquad (71)$$

$$2\eta f_1 \frac{dg_3}{d\eta} - 4f_1 g_3 - \frac{u_2 f_3}{f_1} F_1 + \left[\sigma_4 + (r_1^2 + 2r_2) F_1 + 2r_1 F_2 + F_3\right] = 0 \qquad (72)$$

As viscosity does not influence the radiative transfer directly, Eqs. (53), (54), (55), (58), (59), (60), (63), (64), and (65) are applicable in the inviscid model.

The boundary conditions for the inviscid equations are:

at wall: $A_{i,j} + 2Q_{i,j} = 0 \quad i = 1,2,3 \quad j = 1,2,3$

at shock: $f_1 = f_2 = f_3 = 1 \quad g_1 = 1 \quad g_2 = g_3 = 0 \qquad (73)$

$A_{i,j} - 2Q_{i,j} = 0 \quad i = 1,2,3 \quad j = 1,2,3$

2.4 METHOD OF SOLUTION

2.4.1 Viscous

From Eqs. (51) to (55), we observe that it is convenient to transform the variable from η to ω by

$$\frac{d\eta}{d\omega} = f_1 \tag{74}$$

Equation (74) is solved subject to the condition $\omega = 1$ at $\eta = 1/2$ and $\omega = \omega_o$ at $\eta = 0$. The ω_o is determined from Eq. (74). It is also convenient to stretch the coordinate by $\bar{\omega} = 1/\sqrt{\lambda}\ \omega$ where $\lambda = N/\varepsilon Re$. To retain Eq. (74), the η coordinate is also stretched by $\bar{\eta} = 1/\sqrt{\lambda}\ \eta$. From here on we will use the stretched coordinates but omit the (-) for simplicity. In the ω variable, a formal solution can be obtained for f_1, g_1, A_1's and Q_1's as follows.

The first order energy equation (Eq. 52) can be written in terms of the new variable ω as

$$2\eta \frac{dg_1}{d\omega} + \frac{1}{Pr} \frac{d^2 g_1}{d\omega^2} + F_1(g_1) = 0 \tag{75}$$

A solution of Eq. (75) can be written as (subject to the boundary conditions $g_1(\omega_o) = g_b$ and $g_1(1/\sqrt{\lambda}) = 1$)

$$g_1(\omega) = g_b - Pr\ G_2(\omega) + m_1 G_3(\omega) \tag{76}$$

with $$G_2 = \int_{\omega_o} e^{-G_1} d\omega \int_{\omega_o} F_1 e^{G_1} d\omega$$

$$G_3 = \int_{\omega_o} e^{-PrG_1} d\omega$$

$$G_1 = 2 \int_{\omega_o} \eta \, d\omega$$

$$m_1 = \frac{1 + Pr\, G_2(\frac{1}{\sqrt{\lambda}}) - g_b}{G_3(\frac{1}{\sqrt{\lambda}})}$$

where g_b is the wall enthalpy.

The first order momentum equation (Eq. 51) can be written in the new variable ω as

$$\frac{d^2 f_1}{d\omega^2} + 2\eta \frac{df_1}{d\omega} - f_1^2 + 3\epsilon g_1^{0.84} = 0 \qquad (77)$$

We now differentiate Eq. (77) with respect to ω to obtain

$$\frac{d^3 f_1}{d\omega^3} + 2\eta \frac{d^2 f_1}{d\omega^2} + 3\epsilon \frac{d}{d\omega}(g_1^{0.84}) = 0 \qquad (78)$$

The solution to Eq. (78) can be formally written as

$$f_1(\omega) = 6\epsilon[\omega\, G_5(\omega) - G_6(\omega)] - 3\epsilon[\omega\, G_7(\omega) - G_8(\omega)] + m_2(\omega - \omega_o) \qquad (79)$$

with $$G_4 = e^{-G_1} \int_{\omega_o} \eta g_1^{0.84} e^{G_1} d\omega'$$

$$G_5 = \int_{\omega_o} G_4 \, d\omega$$

$$G_6 = \int_{\omega_o} \omega G_4 d\omega$$

$$G_7 = \int_{\omega_o} g_1^{0.84} \, d\omega$$

$$G_8 = \int_{\omega_o} \omega g_1^{0.84} \, d\omega$$

$$m_2 = 1 + 3\epsilon \left[\frac{1}{\sqrt{\lambda}} G_7 \left(\frac{1}{\sqrt{\lambda}}\right) - G_8 \left(\frac{1}{\sqrt{\lambda}}\right)\right] - 6\epsilon \left[\frac{1}{\sqrt{\lambda}} G_5 \left(\frac{1}{\sqrt{\lambda}}\right) - G_6 \left(\frac{1}{\sqrt{\lambda}}\right)\right] / \left(\frac{1}{\sqrt{\lambda}} - \omega_o\right)$$

The boundary conditions used for Eq. (79) are

$$f_1(\omega_o) = 0, \; f_1\left(\frac{1}{\sqrt{\lambda}}\right) = 1, \; \left.\frac{d^2 f_1}{d\omega^2}\right|_{\omega_o} = -3\epsilon g_b^{0.84}$$

A formal solution for the radiative transfer equations (Eqs. (53) to (55)) can also be obtained. For example, in the first band (i = 1), the radiative transfer equation can be written as

$$\frac{dQ_{1,1}}{d\tau_1} = - A_{1,1} + 4\pi \frac{B_{1,0}}{\alpha_{1,0}}$$

$$\frac{dA_{1,1}}{d\tau_1} = - 3Q_{1,1} \tag{80}$$

where

$$\tau_1 = \sqrt{\lambda}\ \lambda_1 \int_{\omega_o} \alpha_{1,0}\alpha_{1,1} d\omega$$

The solutions to Eqs. (80) subject to boundary conditions of Eq. (66) are

$$Q_{1,1} = C_1 e^{\sqrt{3}\tau_1} + C_2\ e^{-\sqrt{3}\tau_1} + 2\pi(\mathcal{L}_1+\mathcal{L}_2)$$

$$A_{1,1} = - \sqrt{3}(C_1 e^{\sqrt{3}\tau_1} - C_2 e^{-\sqrt{3}\tau_1}) - 2\sqrt{3}\pi(\mathcal{L}_1-\mathcal{L}_2) \tag{81}$$

with

$$\mathcal{L}_1 = e^{\sqrt{3}\tau_1} \int_{\omega_o} \frac{B_{1,0}}{\alpha_{1,0}}\ e^{-\sqrt{3}\tau_1}\ d\omega$$

$$\mathcal{L}_2 = e^{-\sqrt{3}\tau_1} \int_{\omega_o} \frac{B_{1,0}}{\alpha_{1,0}}\ e^{\sqrt{3}\tau_1}\ d\omega$$

and

$$C_1 = - \left(\frac{2+\sqrt{3}}{2-\sqrt{3}}\right) C_2$$

$$C_2 = \frac{2\pi\left[\mathcal{L}_1\left(\frac{1}{\sqrt{\lambda}}\right) + (2 - \sqrt{3})^2\ \mathcal{L}_2\left(\frac{1}{\sqrt{\lambda}}\right)\right]}{(2+\sqrt{3})^2 e^{\sqrt{3}\ \tau_1\left(\frac{1}{\sqrt{\lambda}}\right)} - (2-\sqrt{3}) e^{-\sqrt{3}\ \tau_1\left(\frac{1}{\sqrt{\lambda}}\right)}}$$

Similar solutions can be obtained for the second and third bands.

The solutions to the first term of the series expansion are then given by Eqs. (76) to (81). In order to evaluate these functions, however, initial $f_1(\omega)$ and $g_1(\omega)$ profiles must be assumed. Hence, the solution technique requires a double iteration. A $g_1(\omega)$ profile is first assumed. A $f_1(\omega)$ profile is then assumed and an ω_o determined from Eq. (74). Utilizing this ω_o, a new $f_1(\omega)$ profile is obtained from Eq. (79). A $f_1(\omega)$ and ω_o solution is therefore obtained when the $f_1(\omega)$ profile converges from an iteration of the above procedure. Based upon the ω_o and the converged $f_1(\omega)$, a new $g_1(\omega)$ is calculated from Eqs. (76) and (81). The solution is obtained when $g_1(\omega)$ converges to $\pm$ 3%.

For second and third terms of the series, i.e. f_2, f_3, g_2, g_3, no formal solution can be written. The differential equations can be written in simplified form such that they are numerically integrated from the wall (at ω_o) by guessing values of $df_2/d\omega$, $df_3/d\omega$ at the wall and $g_2(\omega)$, $g_3(\omega)$ until the boundary conditions at the shock are satisfied. The radiative transfer equation can still be solved formally, the form of the solutions are similar to that of Eqs. (81).

2.4.2 Inviscid

In Eqs. (67-72) it is convenient to transform the variable from η to ω as defined by Eq. (74). The resulting equations can be numerically integrated subject to the boundary conditions at the shock (Eq. 72). A problem arises

near the wall in that the solution becomes indeterminant as η approaches zero. Considering the first order equations, the solutions of f_1 and g_1 are obtained by the following iterative technique. A $g_1(\omega)$ profile is assumed and the radiation field obtained from Eqs. (81).* Equations (67, 68, 74) are then numerically integrated to obtain ω_o, f_1 and g_1. As the gas at the stagnation point, $\eta = 0$, is in radiative equilibrium, a $g_1(\omega_o)$ is determined such that the flux divergence, F_1 is zero at the wall. An $f_1(\omega_o)$ is obtained from Eq. (67) such that the velocity gradient is bounded at the wall. A solution is obtained when the iteration on $g_1(\omega)$ converges to $\pm$ 3%.

Solutions for the second and third terms of the series, g_2, f_2, g_3 and f_3, are obtained in a similar manner. As ω_o is determined in the first order solution, the indeterminant nature of the higher order equations is avoided by integrating to $\omega_o + \Delta\omega$ ($\eta = 10^{-4}$).

Once f's and g's are determined, we can find the density from Eqs. (19b) as

$$\frac{1}{\rho} = e g_1^{0.84}[1 + \sigma_1 \xi^2 + \sigma_2 \xi^4] \qquad (82)$$

where σ_1 and σ_2 are given in Appendix I.

The physical normal distance $y(\omega)$ is then given by the transformation Eq.

---

*Note that $\lambda = 1.0$ for the inviscid solution.

(13), namely

$$y = \int_o \frac{r_s^2 d\eta}{\rho u r} \simeq r_s \int_o^\eta \frac{d\eta}{\rho u} \tag{83}$$

and the shock location $\Delta(\xi)$ can be obtained by evaluating Eq. (77) at $\eta = 1/2$. Also, from transformation Eq. (13), we obtain

$$\rho v = - \left[2\eta \frac{dr_s}{d\xi} + r_s \left(\frac{\partial \eta}{\partial \xi}\right)_y \right] \tag{84}$$

where $\left(\frac{\partial \eta}{\partial \xi}\right)_y$ denotes differentiating η with respect to ξ at constant y.

For the viscous case, the convective heating to the wall and the skin friction are also of interest. The skin friction can be written (normalized by $\rho_\infty U_\infty^2$)

$$\tau \text{ Re} = \left(\mu \frac{\partial u}{\partial y}\right)_{\omega_o} \tag{85a}$$

After using Eqs. (74) and (83), we obtain

$$\tau \text{ Re} = \frac{N \rho_s \mu_s}{r_s \sqrt{\lambda}} \left(\frac{u}{f_1} \frac{\partial u}{\partial \omega}\right)_{\omega_o} \tag{85b}$$

$$\tau = \frac{\sqrt{\lambda}\, \mu_s\, \xi}{1 + r_1 \xi^2 + r_2 \xi^4} \left[\left(1 + u_1 \frac{f_2}{f_1} \xi^2 + u_2 \frac{f_3}{f_1}\right)\left(\frac{df_1}{d\omega} + u_1 \frac{df_2}{d\omega} \xi^2 + u_2 \frac{df_3}{d\omega} \xi^4\right) \right]_{\omega_o}$$

In Eq. (85b), we have taken $\rho_s = \text{const} = \frac{1}{\epsilon}$. Convective heating to the wall

(normalized by $\frac{1}{2}\rho_\infty U_\infty^2$) is given by

$$\dot{q} = \frac{\sqrt{\lambda}}{Pr} \frac{\mu_s}{(1 + r_1\xi^2 + r_2\xi^4)} \left(1 + u_1 \frac{f_2}{f_1}\xi^2 + u_2 \frac{f_3}{f_1}\xi^4\right)\left(\frac{dg_1}{d\omega} + \frac{dg_2}{d\omega}\xi^2 + \frac{dg_3}{d\omega}\xi^4\right)_{\omega_o} \tag{86b}$$

In order to solve the energy and momentum equations by the series expansion methods presented in this section, it was necessary to expand the radiative flux in a series form (Eq. 45). Series solutions for a wide range of flight conditions indicated that the radius of convergence for the velocity and enthalpy series was significantly larger than the radius of convergence for the radiative flux series. This problem has been noted by others (Ref. 7) who have solved for the radiative heat flux by series expansion. (This will be discussed in more detail in the results section.) The reason for this appears to be associated with the difficulty in approximating an exponential function with a large argument by a finite series. This expansion is discussed in Appendix III.

In order to avoid this difficulty, the radiative flux is calculated directly from the full radiative transfer and intensity equations. We can see from Eqs. (17) and (18), ξ does not appear explicitly in these equations; therefore, they can be considered as ordinary equations with ξ as a parameter. Hence, once the series solution to the enthalpy profile is obtained, the corresponding radiative flux and intensity can be determined. The second and third order radiative flux solutions (that will be

discussed) therefore correspond to the solution of the radiative transfer equation with the respective second and third order enthalpy profiles.

The solution to Eqs. (17) and (18) are given as (similar to Eq. 81)

$$(q_\eta)_i = D_{i,1}\, e^{\sqrt{3}\tau_i} + D_{i,2}\, e^{-\sqrt{3}\tau_i} + \frac{1}{2}\,(\ell_{i,1} + \ell_{i,2})$$

$$(I_o)_i = -\,D_{i,1}\, e^{\sqrt{3}\tau_i} + D_{i,2}\, e^{-\sqrt{3}\tau_i} - \frac{\sqrt{3}}{2}\,(\ell_{i,1} + \ell_{i,2}) \qquad (87)$$

where

$$\ell_{i,1} = e^{\sqrt{3}\tau_i} \int 4\pi\, S_i e^{-\sqrt{3}\tau_i}\, d\omega$$

$$\ell_{i,2} = e^{-\sqrt{3}\tau_i} \int_{\omega_o} 4\pi\, S_i e^{\sqrt{3}\tau_i}\, d\omega$$

$$D_{i,2} = \frac{\ell_{i,1}\left(\frac{1}{\sqrt{\lambda}}\right) + (2 - \sqrt{3})^2\, \ell_{i,2}\left(\frac{1}{\sqrt{\lambda}}\right)}{2\left[(2 + \sqrt{3})^2\, e^{\sqrt{3}\tau_i\left(\frac{1}{\sqrt{\lambda}}\right)} - (2 - \sqrt{3})^2 e^{-\sqrt{3}\tau_i\left(\frac{1}{\sqrt{\lambda}}\right)}\right]}$$

$$D_{i,1} = -\,\frac{2 + \sqrt{3}}{2 - \sqrt{3}}\, D_{i,2}$$

$$\tau_i = \int_{\omega_o} \frac{\alpha_i (1 + r_1 \xi^2 + r_2 \xi^4}{1 + \frac{u_1 f_2 \xi^2}{f_1} + \frac{u_2 f_3 \xi^4}{f_1}}\, d\omega$$

$$S_1 = \frac{B_1}{\alpha_1} \quad , \quad S_2 = B_2 \quad , \quad S_3 = B_3$$

$$B_1 = f(S)$$

and the total q_η and I_o are

$$q_\eta = \sum_{i=1}^{3} (q_\eta)_i \quad , \quad I_o = \sum_{i=1}^{3} (I_o)_i \tag{88}$$

It should be noted that the f_1's, g_1's and ω_o's (which are implicitly involved in α_i's and B_i's) are functions of ω based on the series expansions of q_η and I_o. The results indicate the solutions of f_i's and g_i's are relatively insensitive to the approximation involved in the series expansions of q_η and I_o. The solutions of q_η as given by Eqs. (87) and (88) were found to have the same region of validity as that of the velocity and enthalpy profiles.

2.5 FLIGHT CONDITIONS CONSIDERED

As one of the prime objectives of this investigation was to evaluate the influence of coupling between the momentum and energy transport mechanisms, case runs were selected with flight conditions and body dimensions* applicable to the hyperbolic reentry problem (Ref. 8) which produced the maximum coupling effect. The maximum coupling will occur at the maximum value of the radiation-convection energy parameter Γ (product of inverse Boltzmann number and the optical depth). As the Boltzmann number and optical depth are independent parameters, the flight conditions commensurate with a maximum Γ value for a minimum and maximum value of optical depth were used. In addition to these two extreme radiation cases, a check run was made for free flight conditions

*$11 \le U_\infty \le 18$ km/sec; $10^{-7} \le \rho_\infty \le 10^{-6}$ gm/cm^3; $50 \le R_s \le 300$ cm

currently being investigated as a "standard" hyperbolic reentry case.* A corresponding case of no radiation influence was made for each of the three cases noted and the resulting matrix of six cases were investigated for both viscous and inviscous models. (It is noted that the Reynolds number becomes a dependent parameter when the optical depth and the radiation-convection value Γ are used as independent parameters.) Table 1 is a summary of the parametric conditions of the three cases investigated and Figure 2 (Ref. 9) illustrates the corresponding regions of interest on a thermodynamic properties plot of reentry conditions.

Numerical solutions are obtained by the input of the free flight conditions (velocity and density), stagnation point shock radius, Prandtl number, and the viscous parameter λ for the viscous case ($\lambda = 1$ for the inviscid case). In that the coordinate system used in the formulation was body oriented, an assumed shock shape is required. The shock shape is input through the constants of the parameter series expansion along the shock (Eq. 44). These constants are, for a given body, all a function of the bluntness parameter B_s. (Assuming the shock is conical in shape.) The values of B_s can be found by first assuming a value, then adjusting it to fit the calculated shock shape. First guess values of B_s in this report were taken directly or extrapolated from the curve given in Lomax and Inouye (Ref. 10). No iteration on B_s is carried out in this study.

The computational time on an 1108 computer per solution (three terms) ranged from 1 1/2 minutes for an inviscid case to 4 minutes for a viscous case.

*U_∞ = 16 km/sec; $\rho_\infty = 4.21 \times 10^{-7}$ gm/cm^3; R_s = 234 cm.

TABLE I

PROPERTIES FOR CASES INVESTIGATED

	CASES		
	I	II	III
Free Stream Velocity (km/sec)	16.0	18.0	11.0
Free Stream Density, ρ_∞ ($\times 10^{-7}$ gm/cm^3)	4.21	1.0	10.0
Stagnation Point Shock Radius, R_s (meter)	2.34	0.5	3.00
Normal Shock Density Ratio, ϵ	0.057	0.055	0.065
Reynolds Number, Re ($\rho_\infty U_\infty R_s/\mu_s(o)$)	216,000	18,000	128,000
Viscous Parameter, λ ($\rho_w\mu_w/\rho_s\mu_s\epsilon$Re)	1.56×10^{-3}	3.04×10^{-2}	3.24×10^{-4}
Radiation Cooling Parameter, $\delta(2q_w/\frac{1}{2}\rho_\infty U_\infty^3)$	0.454	0.226	0.015

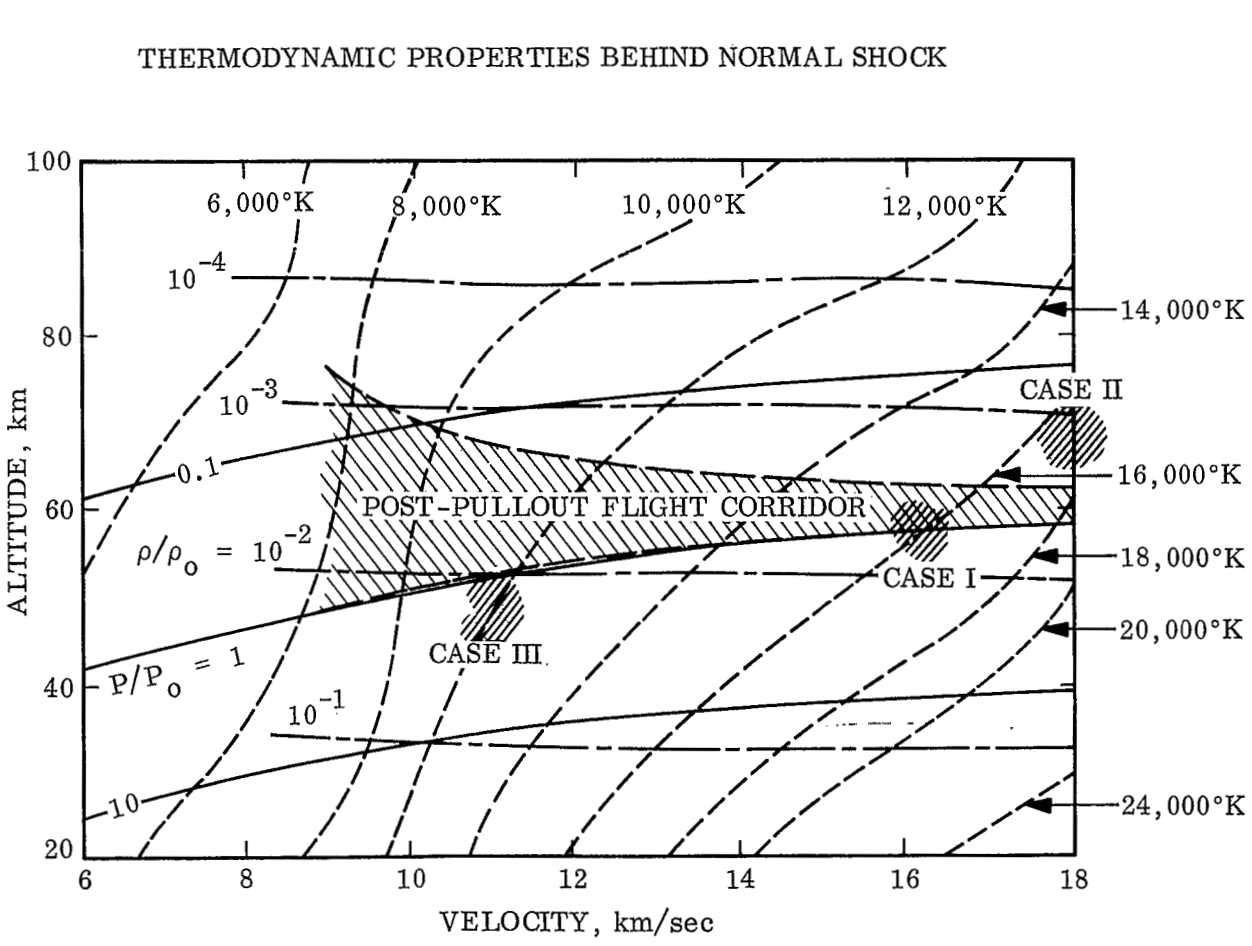

Fig. 2 Free Stream Conditions

Section 3
RESULTS

3.1 VALIDITY OF SERIES SOLUTIONS

The utility of the Blasius type series used in Eqs. (44) and (45) (like any series method) is restricted in that its global accuracy for a finite number of terms can only be evaluated by a comparison with an "exact" solution for a given problem. In this manner, Chou (Ref. 2) showed his closed form Blasius series solution* of the adiabatic inviscid thin shock layer was most effective ($\pm$ 5%) in predicting the gasdynamics about a variety of bodies to the sonic line. For the viscous and inviscid radiating flow of a thin shock layer about a body, no "standard" solutions exist for comparison. The validity of a finite series solution to these radiating flow models may, therefore, only be assessed by indirect arguments.

The same form of series expansions were used in this investigation as was found successful in the adiabatic inviscid solutions of Chou (Ref. 2). As the radiative flux addition to the energy equation influences the gasdynamics only indirectly through the density field, it was anticipated that the radiation flux would affect the gasdynamics of the flow by a perturbation effect. The coupling results discussed later in this section showed this to be true for both the inviscid and viscous models.

---

*Three-term series.

The validity of the series solution for each parameter must rest on two factors: (1) the numerical convergence of the series solution, and (2) the physical interpretation of the results. Consequently, the region of numerical convergence of the enthalpy series and the corresponding radiative energy flux are discussed.

Figure 3 illustrates the numerical convergence of the enthalpy profile at two different body angles. At 44°, the deviation from second to third term is approximately 20%. The results of applying Shanks nonlinear transformation (Ref. 11) to the first three terms in the series are given. The Shanks formation represents an approximate method of predicting the converged solution of a series expansion given three or more terms of the series. This transformation technique has been frequently utilized by Van Dyke et al. (Refs. 12, 13) as an indication of the rate of series convergence. A comparison of the Shanks results with the third term solution indicates that a three term expansion is effective in describing the enthalpy field to a body angle of 44°.

The numerical convergence of the radiative and convective energy fluxes to the wall is shown in Fig. 4. Results from two methods of calculation of the radiative energy flux are indicated. The series solution was initially used; however, the physically impossible nature of the second order series results of the radiative energy flux results beyond 35° indicates a serious breakdown of the flux series beyond this point. The slow convergence indicated by the discrepancy between the second and third order terms suggests that several additional terms are required in order to obtain a solution valid near the sonic

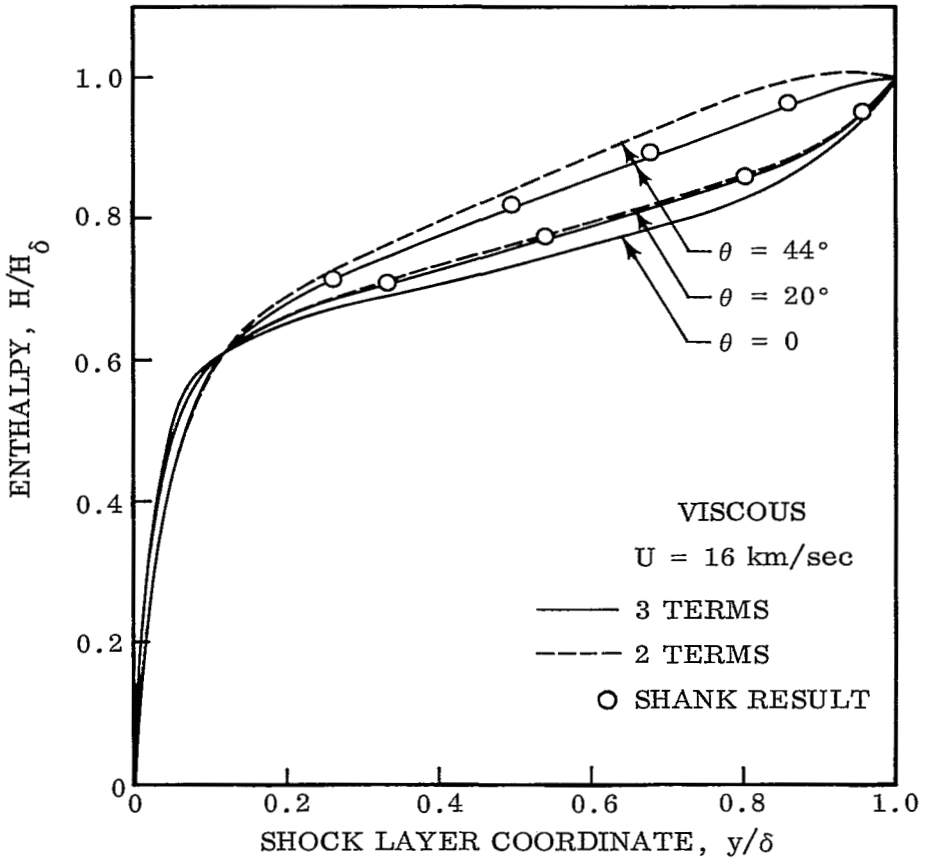

Fig. 3 Numerical Convergence of Enthalpy Distribution ($\theta = 20^{o}, 44^{o}$)

line. This slow numerical convergence of the radiative heat flux series was also noted by Cheng (Ref. 7). Cheng suggested the convergence could be improved by a change in the form of the radiative heat flux series expansion. (This has not been shown valid.) Because of the rapid convergence of the enthalpy series as shown by Fig. 3, the radiant flux was obtained in this investigation from a solution of the complete transfer equation (the differential approximation) once the enthalpy distribution was calculated. The improved numerical convergence of the radiative flux by this method is shown in Fig. 4. The results from the Shanks enthalpy distribution indicate the three-term solution to be a valid solution to the sonic line ($\sim 44^{\circ}$).

As the convergence of the convective heat flux series is directly proportional to the enthalpy results at the wall, Fig. 4 shows the radius of convergence of the convective flux series (Eq. 86b) to be very large. Figures 3 and 4 are illustrative of the results of the three cases investigated. They show the three term series solution numerically converges to the Shanks results ($\pm$ 5%) to a body angle near the sonic line ($\sim 45^{\circ}$).

Figure 5 shows the comparison of the stagnation point enthalpy results of the viscous and inviscid series solutions with the detailed viscous code (VISC) (Ref. 1). Slight discrepancies between the series solutions and the VISC results are noted. The deviation of results in the boundary layer is attributed to the constant Prandtl number value of .77 used in the series solution. This constant value infers a higher fluid conductivity in the boundary layer than the temperature dependent Prandtl number associated with air at high temperatures

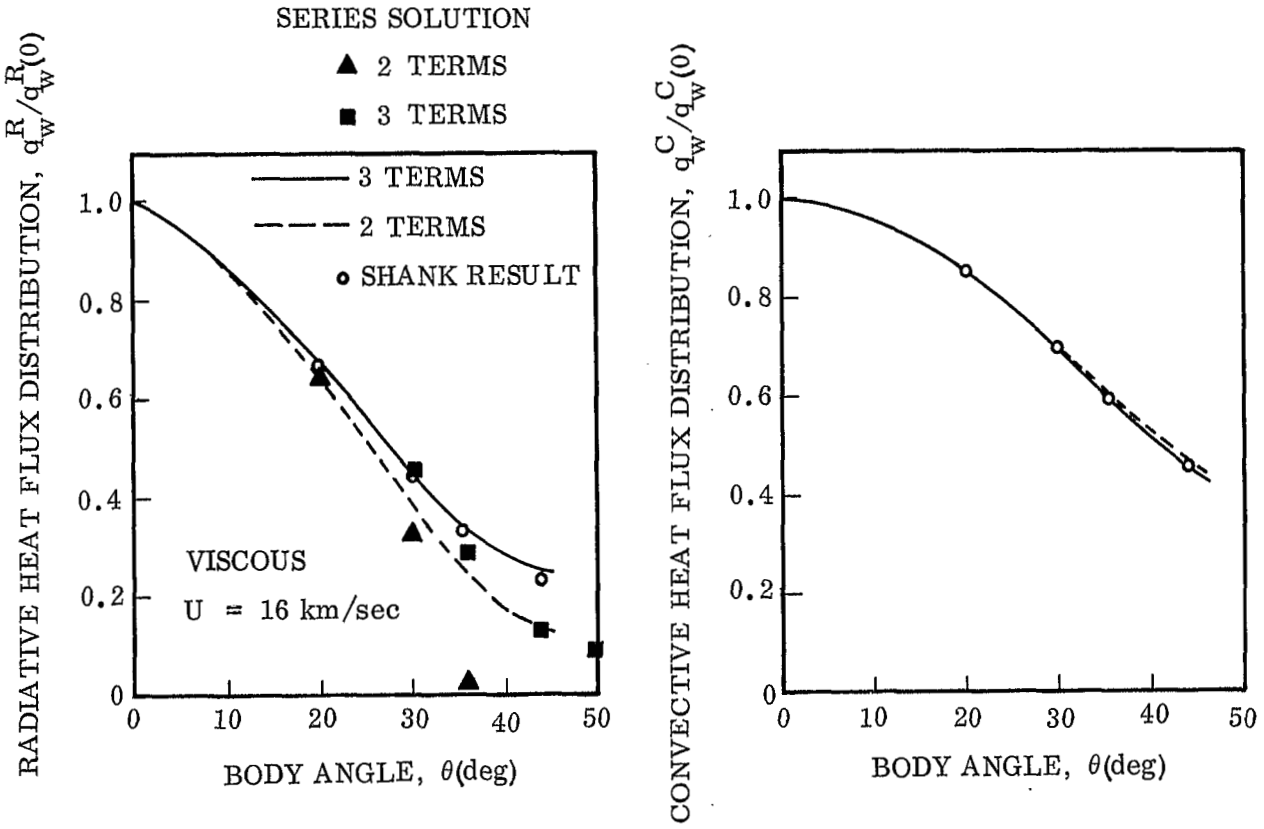

Fig. 4 Numerical Convergence of Radiation and Convective Heat Fluxes

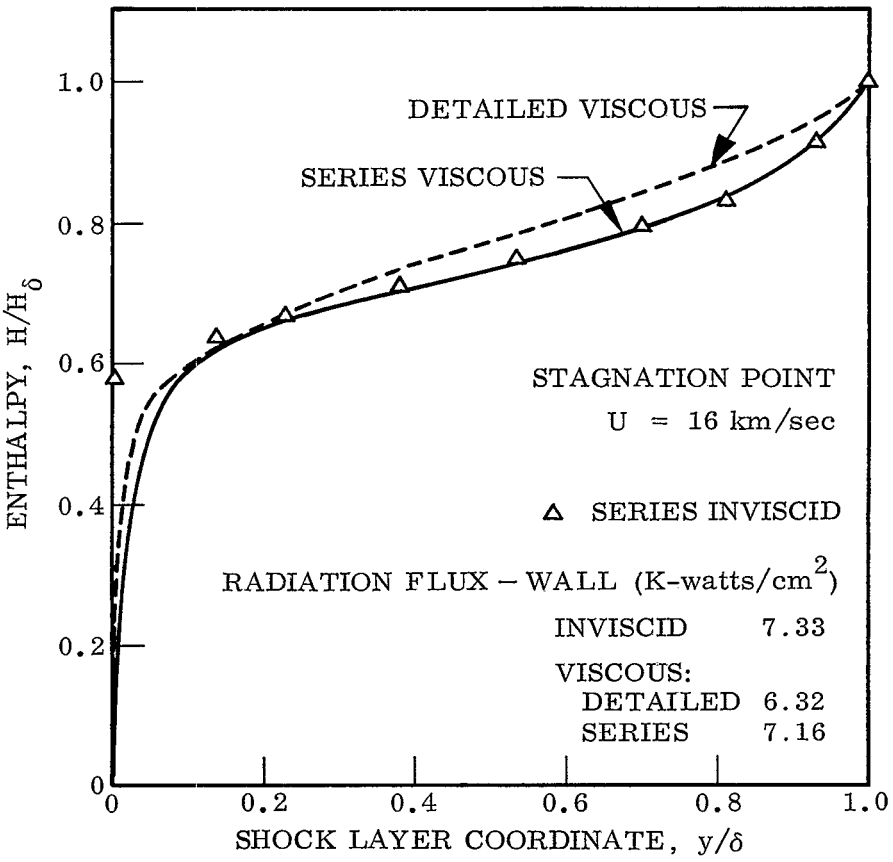

Fig. 5 Comparison of Stagnation Point Enthalpy Distributions and Radiative Fluxes

(Ref. 14). Consequently a thicker boundary layer is experienced by the series solution. The reason for the deviation of the enthalpy profiles in the inviscid region is not clearly understood. It is noted, however, that the analytical equation of state used in the series solution results in an enthalpy-temperature relationship which is independent of pressure. Comparisons with VISC code showed small resulting temperature differences. Because of the strong temperature dependence of the absorption and emission terms, however, small temperature differences are sufficient to influence the radiative transfer significantly. This suggests that an improvement in the series solution should include a more precise equation of state.

It should be recalled that the prime motivation for the series solution method was to determine the degree of coupling between the momentum and energy transport mechanisms. The numerical convergence results of Figs. 3 and 4 and the comparison of the stagnation point results of Fig. 5 justify the validity of the series expansion solutions to this end.

The nature of the enthalpy and velocity distribution through the shock layer for different body angles is shown in Fig. 6. For the inviscid region the increase of the total enthalpy away from the stagnation point results from the expected increase in velocity and decrease in radiative heat loss of the flow as it leaves the stagnation region. The conductivity in the boundary layer increases the boundary layer thickness and correspondingly decreases the convective heat flux.

The negligible variation of the velocity profiles about the body as shown in

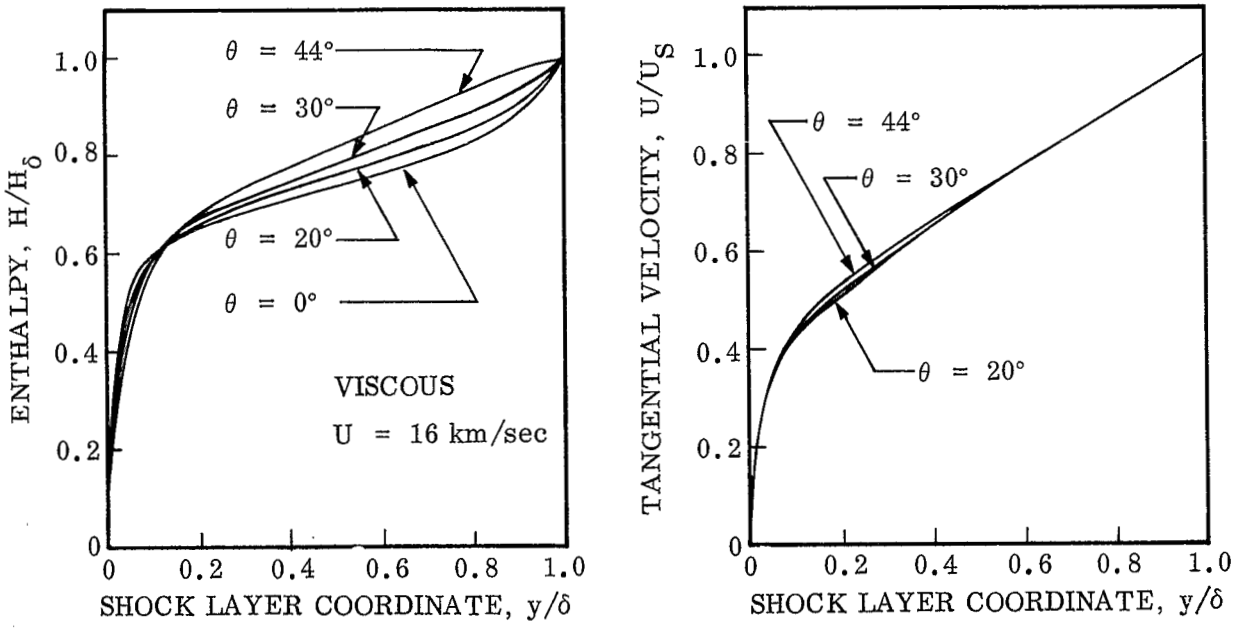

Fig. 6 Characteristic Enthalpy and Velocity Distributions Versus Body Angle

Fig. 6 were found to be very interesting. This is due to the rapid numerical convergence of the velocity series (Eq. 45). This insensitivity to body angle suggests the coupling from the enthalpy distribution to the momentum field is weak. This coupling will be discussed further in the results section.

The convective and radiative heat flux distribution about a body are shown in Fig. 7. As was noted by Hoshizaki and Wilson (Ref. 5) the radiative heating decreases significantly more rapidly than the convective heating. However, the radiative heat flux is approximately 25% of its stagnation point value at the sonic line.

Figure 8 illustrates an assumed and calculated shock shape. Since the primary objective of this report is to study the various coupling effects between flow field and radiation field rather than to give an accurate quantitative result for radiating thin shock layer, an iteration on shock shape was not carried out in this investigation.

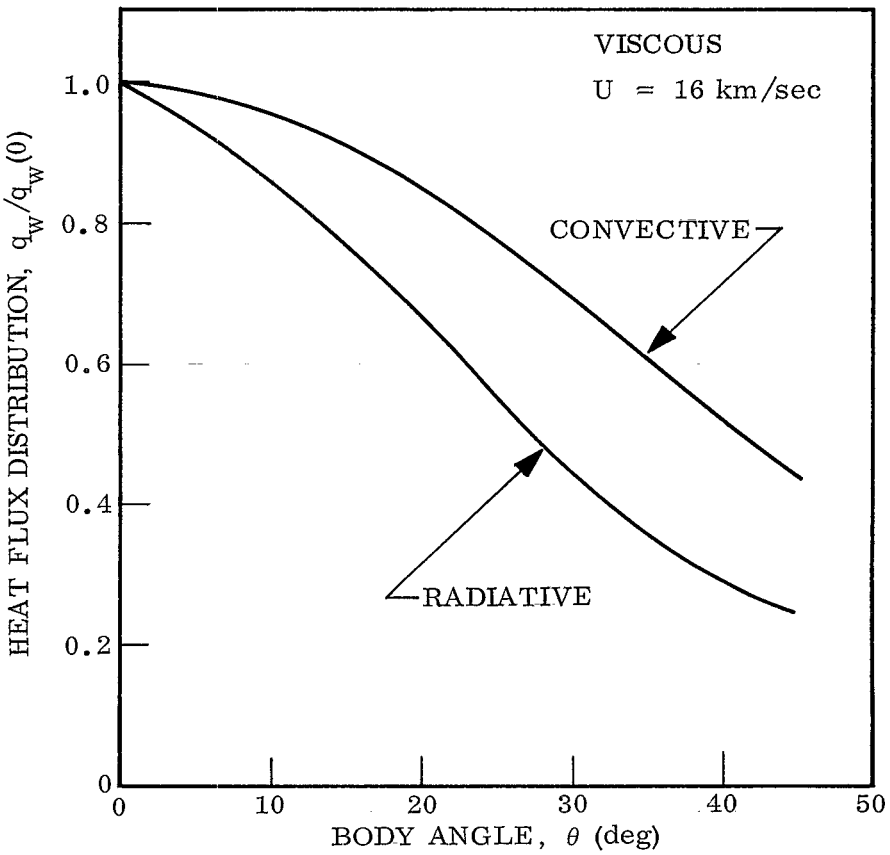

Fig. 7 Characteristic Radiative and Convective Heat Fluxes Versus Body Angle

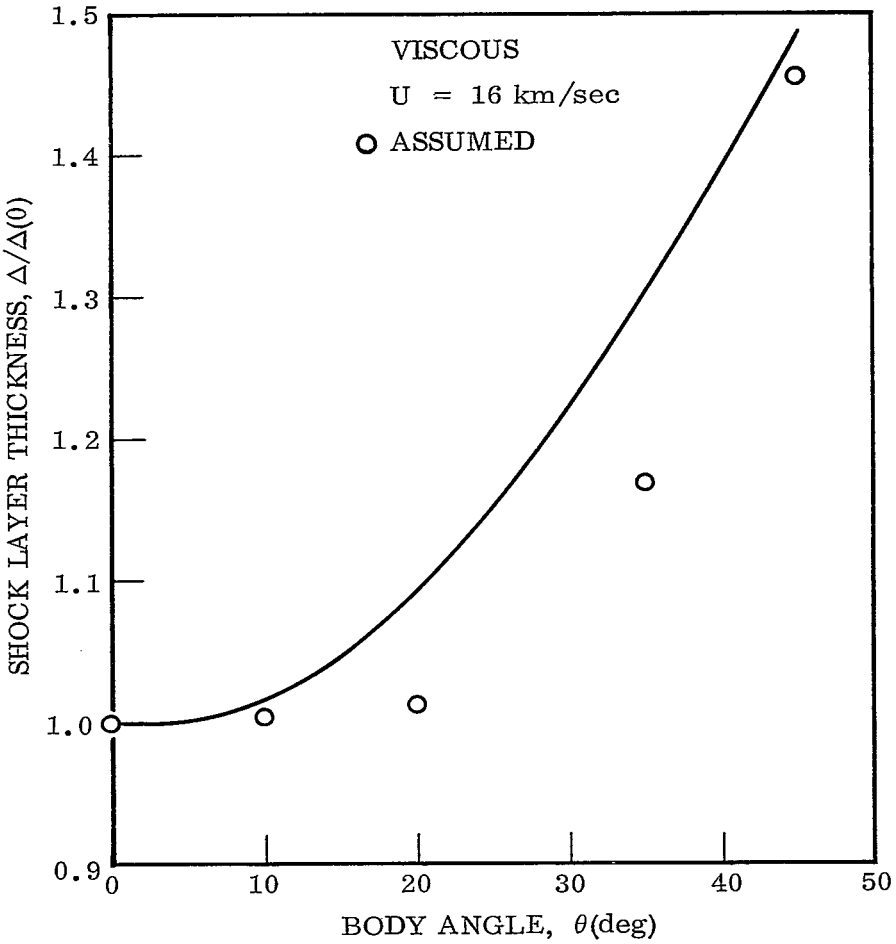

Fig. 8 Calculated and Assumed Shock Shape

3.2 COMPARATIVE RESULTS

A comparison of the enthalpy, velocity and heat flux results for the three flight conditions* considered (Table 1) is presented in Figs. 9 and 10. The relative effects of the three flight conditions upon the resulting enthalpy and velocity profiles in the shock layer and the heat flux distribution at and away from the stagnation point will be considered.

Illustrative enthalpy and velocity results are shown in Fig. 9. The results presented are for a representative body angle of 36° for both the viscous and inviscid models. The magnitude of radiative and viscous transport govern the enthalpy and velocity distributions. Although radiative transport will thicken the boundary layer somewhat, the general boundary layer distribution is a direct function of the magnitude of viscosity. (Note, however, the thick gas effect near the wall of the 11 km/sec inviscid case.) Comparing the magnitudes of the viscous parameters in Table 1 for the three cases, the largest viscous influence is anticipated for the 18 km/sec case. This is substantiated by the enthalpy and velocity boundary layer profiles noted in Fig. 9. The 16 and 11 km/sec cases have significantly less viscous influence as is demonstrated by their decreased boundary layer thicknesses. Correspondingly, the viscous velocity profiles of the latter two cases differ only slightly from the inviscid runs near the wall.

The significant influence of the radiative transport is observed in the inviscid

*In this discussion, the free flight velocities are used as the identification of the three cases considered.

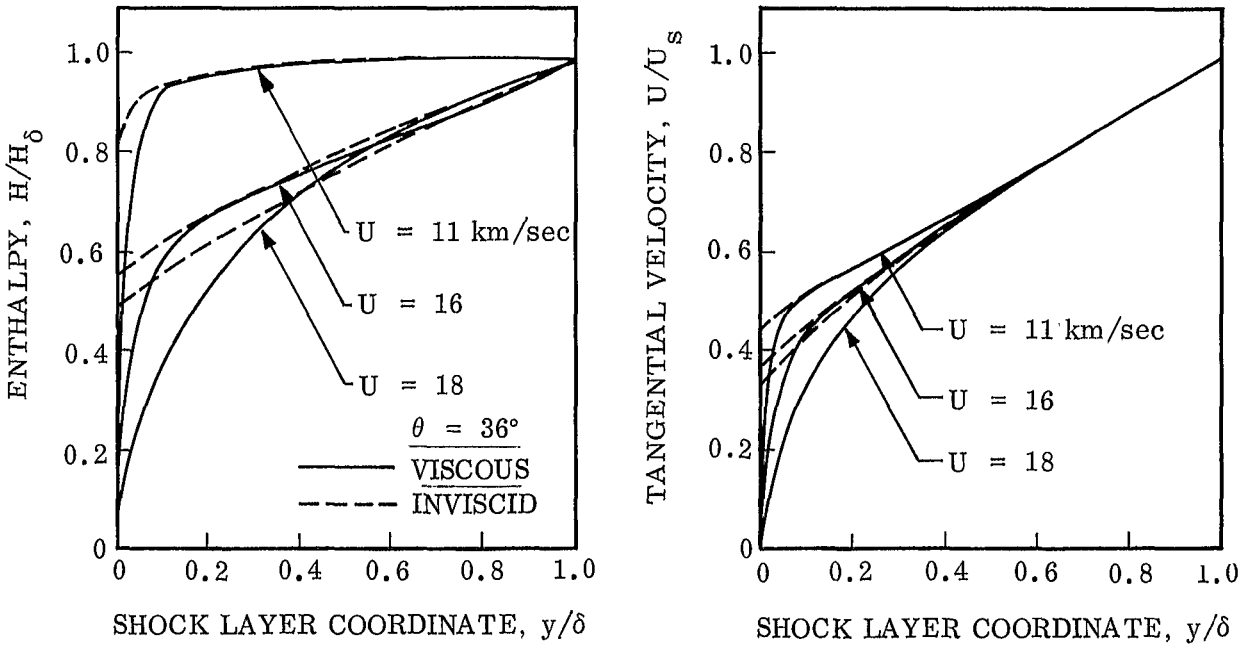

Fig. 9 Enthalpy and Velocity Distributions For Three Stream Cases ($\theta = 36^\circ$)

region of the enthalpy distributions. Having comparable cooling parameters, Γ, the 16 and 18 km/sec cases experience similar enthalpy profiles in the inviscid region. In contrast, the small cooling parameter of the 11 km/sec case results in an enthalpy profile approaching that of an adiabatic flow.

The conformity of the velocity results in the inviscid region indicates the influence of the radiative transport upon the velocity field is small. This coupling will be discussed in detail in subsequent paragraphs of this section.

Figure 10 illustrates the relative comparison of the convective and radiative heat fluxes about the body. The differences in the distributions demonstrate the significance of the free stream condition upon the convective and radiative heat loads about the body. The radiative flux is a direct function of the temperature level in the shock layer. At high temperatures, the radiative properties of emission and absorption are less sensitive to temperatures than at the lower temperature levels. Consequently, even though the temperature change in the shock layer away from the stagnation point is the

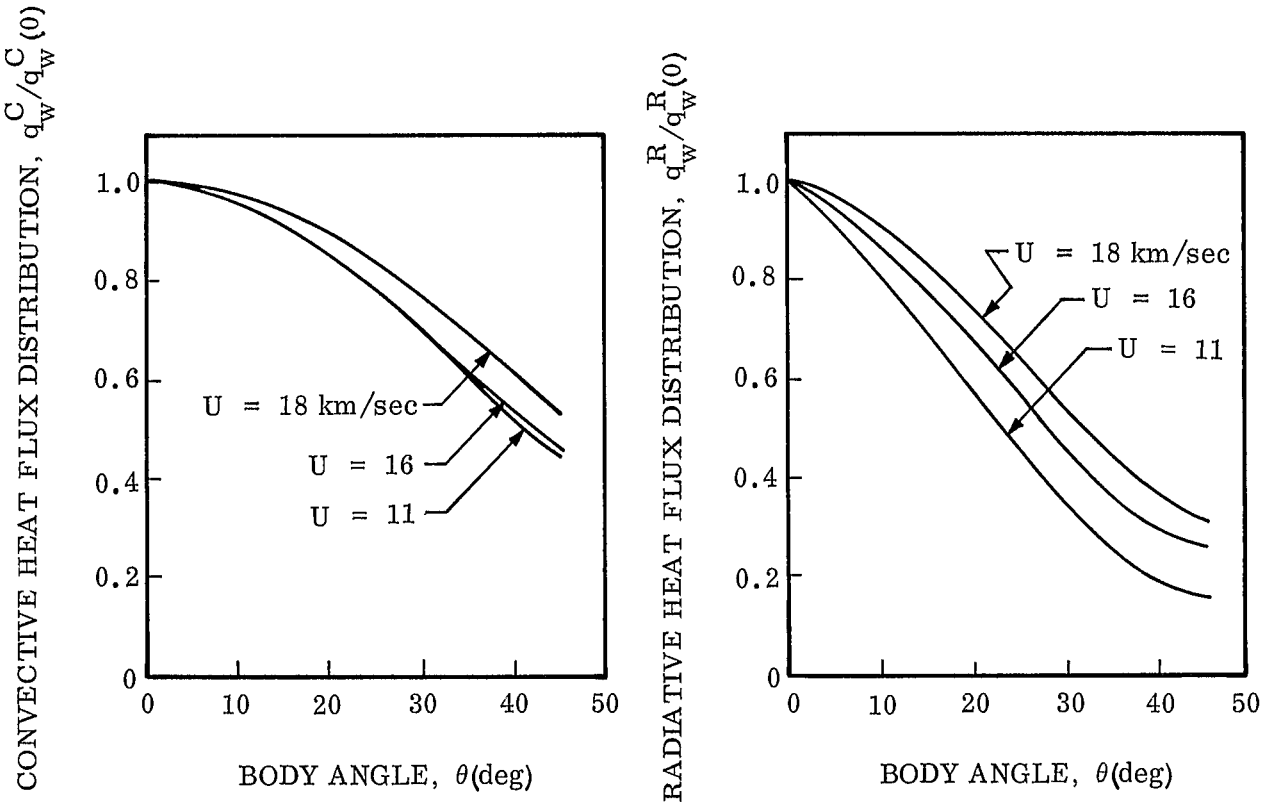

Fig. 10 Convective and Radiative Heat Flux Distributions for Three Free Stream Cases

greatest in the high velocity case* (18 km/sec), the change of radiative heat flux about the body for this case is the least for the three considered. In the 11 km/sec case, the temperature change about the body is the least, however, the temperature level is sufficiently low that a small temperature change results in a significant influence upon the radiative properties. This is demonstrated by the correspondingly large radiative flux change for this case about the body as shown in Fig. 10.

The thickening of the enthalpy boundary layer away from the stagnation point accounts for the general decrease in convective heating. The relative convective heating distributions compare with the respective gradients of the enthalpy profiles of Fig. 9 at the wall. The 11 and 16 km/sec cases experience essentially the same convective heating while the large viscous influence of the 18 km/sec case produces a marked change from the other two. Because of the strong temperature dependence of the radiative flux, the change in radiative flux about the body is more pronounced for all cases than the corresponding changes in convective heating. Due to the high radiative heat flux experienced at the stagnation point of a blunt body, however, the radiative heating is far from negligible at the sonic line.

3.3 MOMENTUM AND ENERGY COUPLING

An understanding of the degree of coupling between the momentum and energy transport mechanisms was the prime objective of this investigation. Such an

*Because of the low velocity at the stagnation point, the stagnation point temperature is a direct function of the free stream velocity.

understanding could provide the justification for simplifying approximations in obtaining solutions of the radiating flow about a body. Such approximations would be essential should detailed treatment of the radiative and collisional transport be required.

The comparison of the radiative heat fluxes for both viscous and inviscid models away from the stagnation point for the three cases considered is presented in Fig. 11. The stagnation point radiative heat flux for each case is noted for comparison. As was expected, the inviscid model yielded the higher radiative cooling; however, the difference between the viscous and inviscid models was surprisingly small for all three cases. The influence of viscosity upon the radiation wall flux was only experienced beyond approximately 30°. Being a direct function of temperature, this difference in the radiative fluxes is attributed to the influence of viscosity on the thickening of the boundary layer. As the flow proceeds about the body, a greater portion of the total radiative heat flux comes from the boundary layer region; therefore, the influence of the viscosity is experienced more dramatically far from the stagnation point. The resulting deviations are shown to be significant near the sonic line with the viscous results below the inviscid case as indicated in Fig. 11. Consequently, the primary effects of viscosity on the radiative heat fluxes is beyond a body angle of approximately 40°. In the stagnation region, the inviscid analysis yields an accurate description of the radiative heating for the range of Reynolds numbers and radiative coupling levels studied.

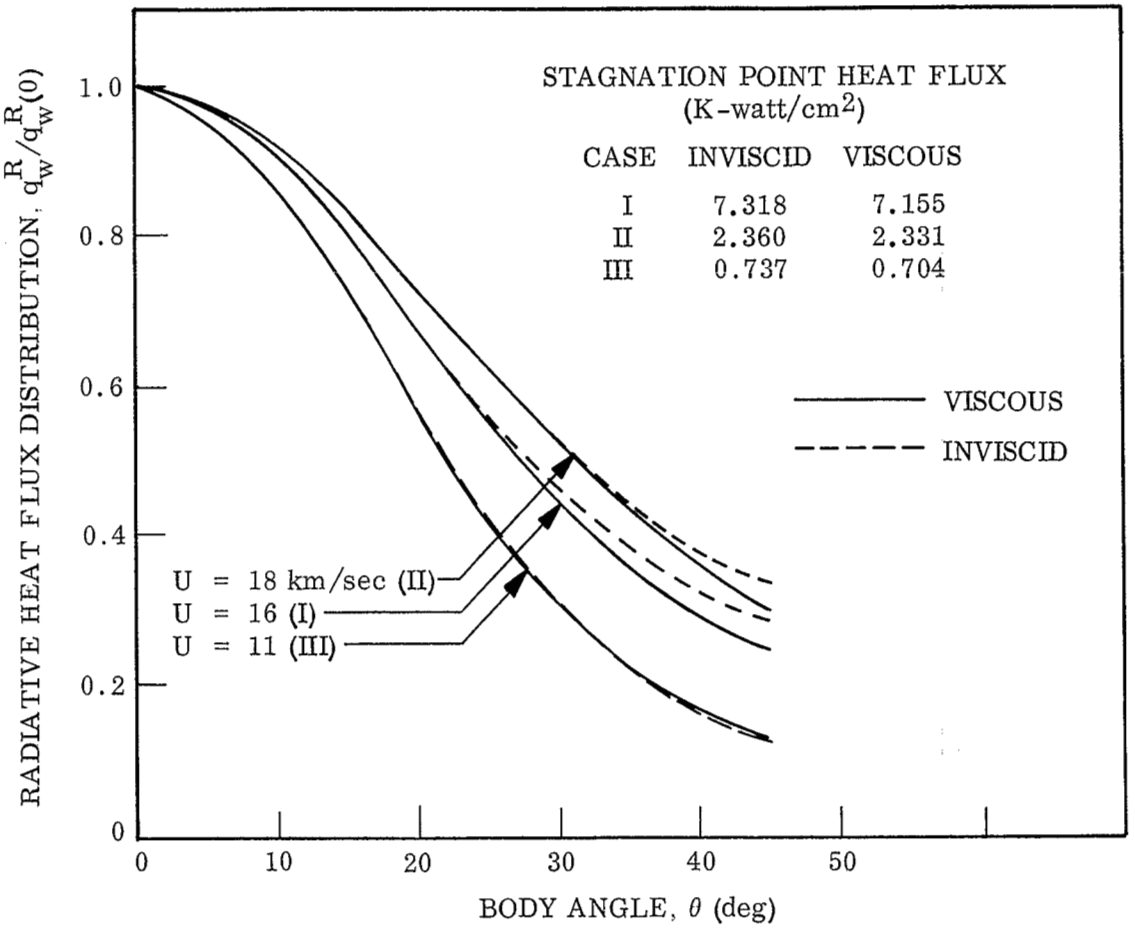

Fig. 11 Coupling of Viscosity and Radiative Heat Flux

The effect of the radiation transport upon the convective heating load about a body is illustrated in Fig. 12. Because of the complexity added to the viscous energy equation by the divergence of the radiative flux, the error produced in the convective flux by its omission is of interest. The stagnation point convective heat flux results show the radiative transport can have an appreciable influence on the convective loss. As one would anticipate, the radiative heat loss thickens the boundary layer resulting in a lowering of the convective losses. Because of the large viscous effect in the 18 km/sec case, this influence is seen to effect this case less than the other two. (The 11 and 16 km/sec results were essentially the same.) Consequently, the results of Figs. 11 and 12 indicate the radiative heat flux determined by neglecting the flow viscosity can overpredict the radiative loss by less than 15%, but an overprediction of 35% in the convective heat flux can be experienced when the radiative transport is neglected in the energy equation.

Figure 13 illustrates the influence of the radiative transport upon the velocity field for both the viscous and inviscid flow models. As the heating load distributions are of prime importance, this coupling is shown indirectly by comparing the influence of two velocity fields upon the radiative heating flux, one from a completely coupled calculation and one from a non-radiating solution. It should be recalled that the momentum transport is only effected indirectly by the energy field through the density. The results shown in Fig. 13 indicate this coupling to be weak at the stagnation point. The "momentum without radiation" results are from the solution of the energy

STAGNATION POINT HEAT FLUX
(K-watt/cm^2)

CASE	RAD	W/O RAD
II	2.33	3.04
III	0.704	0.653

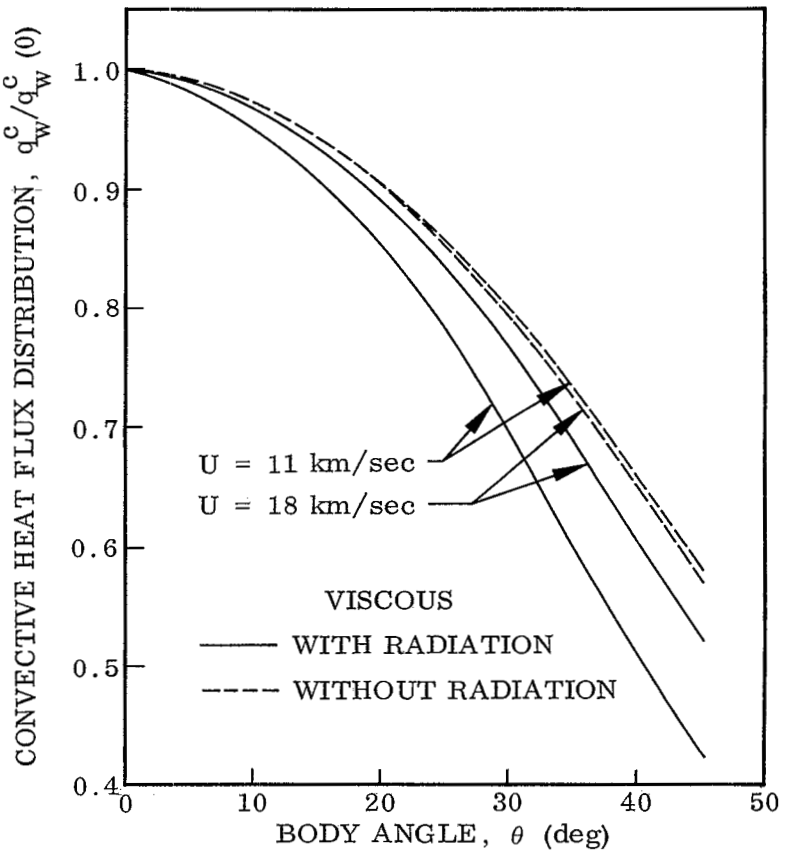

Fig. 12 Coupling of Radiative Transport Convective Heat Flux

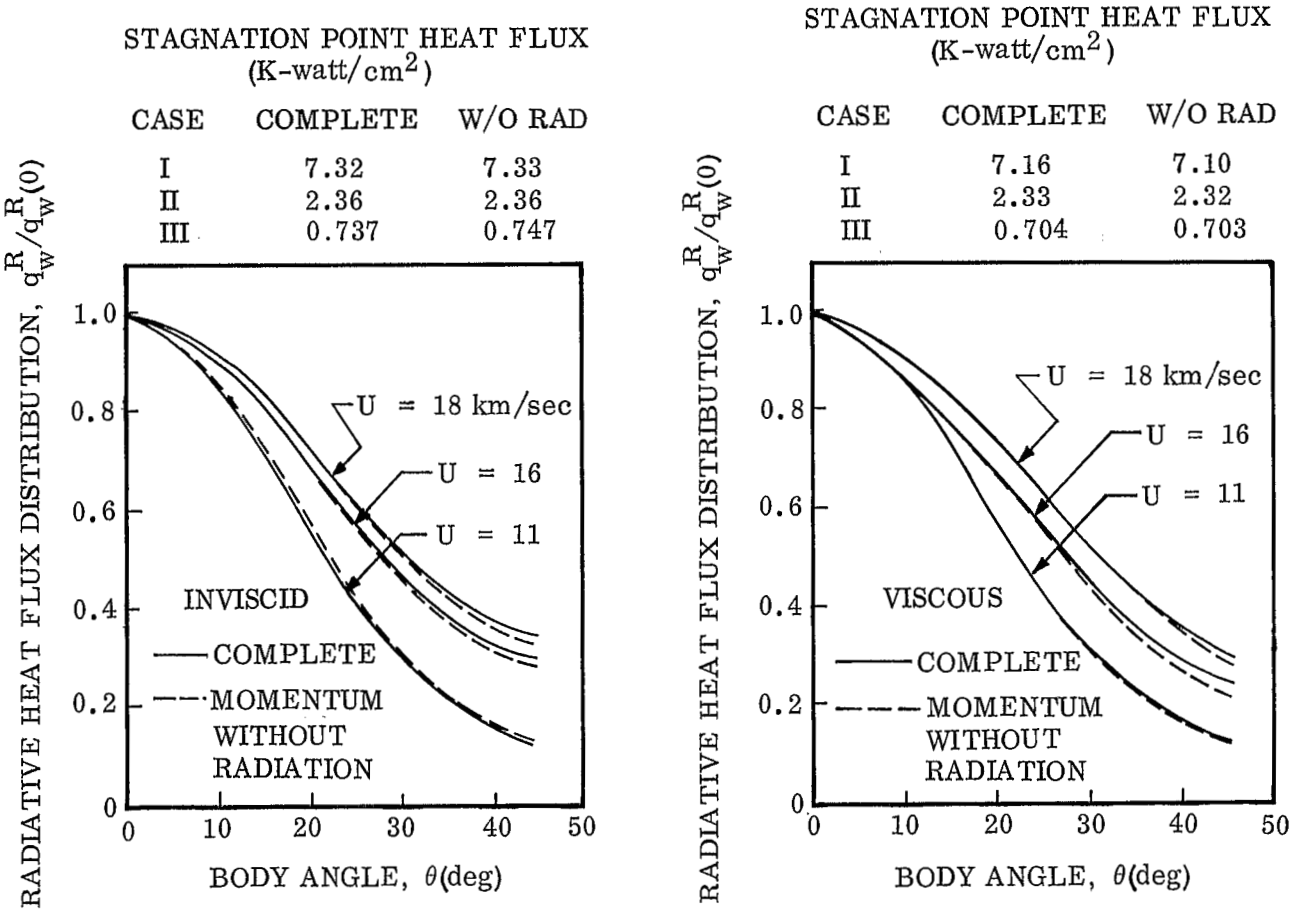

Fig. 13 Coupling of Radiative Transport to the Velocity Field

equation using a solution to the momentum equations obtained from a non-radiating flow calculation. For the inviscid model, this velocity field represents the adiabatic inviscid series solution of Chou (Ref. 2). For the viscous case, the velocity field was determined from a solution of the combined energy and momentum equations without the radiative flux divergence term. The results of Fig. 13 indicate the weak coupling of the radiative transport on the velocity field as the latter influences the radiative flux away from the stagnation point. In connection with the results of Fig. 11, these results indicate that an accurate description of the radiative heat flux can be obtained by the solution of the energy equation using the closed-form adiabatic inviscid velocity distribution of Chou (Ref. 2).

Section 4
CONCLUSIONS

A three-term series formulation of the viscous and inviscid, radiating-absorbing flow in a thin shock layer about an axisymmetrical body has been completed. The radiative transport was modeled with a three band continuum absorption coefficient and was described by the differential approximation. Solutions for each of the three terms in the series have been obtained for a spherical body at three flight conditions which provide a wide variation in the effects of viscosity and radiative cooling. The three term solutions were compared with the results of a Shanks non-linear transformation of the series. Numerical convergence was thus confirmed for the enthalpy and velocity series away from the stagnation point to a body angle near the sonic line. Having obtained an enthalpy distribution, the radiative heat flux was found from the solution of the radiative transport equation since the radiative heat flux series was shown to slowly converge. A comparison of the series solution with a detailed stagnation point calculation showed that the series formulation had properly accounted for the essential physics of the flow.

The radiative and convective heating distributions were obtained to a body angle of 45° for the three cases considered. The coupling between the momentum and energy transport was evaluated by comparisons of the convective and radiative flux distributions at and away from the stagnation point. This coupling analysis indicated that the influence of viscosity on the radiative

heat flux calculation was small (< 15%). The radiative transport was shown to effect the convective heat flux more strongly. The convective heating may be increased by 35% near the sonic line when the radiative transport is neglected. The influence of the radiative transport on the velocity field was shown to be small. The radiative flux results obtained by using a velocity field obtained from a non-radiating flow calculation was shown to agree very closely with the results of the fully coupled analysis.

These results suggest that an accurate description of the radiation heating about a blunt body can be obtained from an uncoupled solution of the energy equation with an adiabatic inviscid description of the velocity field (e.g. Ref. 2).

Section 5
REFERENCES

1. Wilson, K. H., "Stagnation Point Analysis of Coupled Viscous-Radiating Flow With Massive Blowing," Lockheed Missiles & Space Co., NASA CR-1548, Feb. 1970.

2. Chou, Y. S., "Inviscid Hypersonic Flow Past Blunt Bodies," AIAA J. 7, 149, 1969.

3. Chou, Y. S., "Series Solution for Hypersonic Flow Past Blunt Bodies," NASA Rept. CR-1266, February 1969.

4. Vincenti, W. G. and Kruger, C. H. Jr., "Introduction to Physical Gasdynamics," Chap. XII, Wiley & Sons, 1965.

5. Hoshizaki, H. and Wilson, K. H., "Convective and Radiative Heat Transfer During Superorbital Entry," Lockheed Missiles & Space Co. Report 4-43-65-5, June 1966.

6. Neel, C. A. and Lewis, C. H., Interpolation of Imperfect Air Thermodynamics Data," Arnold Engineering Development Center, Rept. AEDC-TDR-64-184, Sept. 1964.

7. Cheng, P. and Vincenti, W. G., "Inviscid Radiating Flow Over a Blunt Body," J. Fluid Mech. 27, 625-646, 1967.

8. Syvertson, C. A., "Entry and Landing Requirements for Manned Planetary Missions," presented at AIAA Technology for Manned Planetary Missions Meeting, New Orleans, La., March 4-6, 1968.

9. Page, W. A., Compton, D. L., Borucki, W. J., Ciffone, D. L., and Cooper, D. M., "Radiative Transport in Inviscid Nonadiabatic Stagnation-Region Shock Layers," AIAA Paper 86-784, June 1968.

10. Lomax, H. and Inouye, M., "Numerical Analysis of Flow Properties About Blunt Bodies Moving at Supersonic Speeds in an Equilibrium Gas," NASA TR R-204, 1964.

11. Shanks, D., "Non-Linear Transformations of Divergent and Slowly Convergent Sequences," J. Math. and Phys. 34, 1, 1955.

12. Van Dyke, M., "Hypersonic Flow Behind a Paraboloidal Shock Wave, J. de Mecanique 4, 477, 1965.

13. Swigart, R. J., "A Theory of Asymmetric Hypersonic Blunt-Body Flows," AFOSR-TN-62-2232, January 1962.

14. Blake, L. H., "Approximate Transport Calculations for High Temperature Air," Lockheed Missiles & Space Co. Report LMSC 6-78-69-20, May 1969.

Appendix I

LIST OF COEFFICIENTS

FIRST ORDER

$$\lambda = N/\epsilon \, Re$$

$$C_2 = 4.47 \times 10^{12} \frac{(kT_{s(o)})}{\rho_\infty U_\infty^3} \quad , \quad C_3 = 2.68 \times 10^{-3} \, (kT_{s(o)})^{3/2} C_2$$

$$\tilde{b} = 2.1 + C_5 T_1 + C_6 T_1^3$$

$$f(a) = e^{-a/T_1} \, (a^3 + 3a^2 T_1 + 6aT_1^2 + 6T_1^3)$$

$$f(b) = e^{-b/T_1} \, (b^3 + 3b^2 T_1 + 6bT_1^2 + 6T_1^3)$$

$$f(aT_1) = e^{-a/T_1} \, (3a^2 T_1 + 12aT_1^2 + 18T_1^3)$$

$$f(bT_1) = e^{-b/T_1} \, (3b^2 T_1 + 12bT_1^2 + 18T_1^3)$$

$$T_1 = g_1^{0.49} \quad , \quad \beta_1 = \left[\frac{C_2 T_1 e^{-\theta_d/T_1}}{1 + C_2 T_1 e^{-\theta_d/T_1}} \right]^{1/2} \quad , \quad \varphi_1 = \left[\frac{C_3 T_1^{5/2} e^{-\theta_i/T_1}}{1 + C_3 T_1^{5/2} e^{-\theta_i/T_1}} \right]^{1/2}$$

$$B_{1,o} = \begin{pmatrix} \beta_1 T_1 e^{-C_4/T_1} \\ T_1 e^{-C_4/T_1} \end{pmatrix}$$

$$B_{2,o} = 1$$

$$B_{3,o} = 1$$

$$B_{1,1} = \begin{pmatrix} 1 \\ 1 - \varphi_1 \end{pmatrix} \tilde{b}$$

$$B_{2,1} = 2T_1 [f(a) - f(b)]$$

$$B_{3,1} = 2T_1 f(b)$$

$$\alpha_{1,0} = \begin{pmatrix} \beta_1 \\ 1 \end{pmatrix} e^{-C_4/T_1} \Big/ \left[\frac{2\pi^4 T_1^3}{15} - 2f(a)\right]$$

$$\alpha_{2,0} = \begin{pmatrix} \beta_1 \\ 1 \end{pmatrix} \frac{e^{-C_7/T_1}}{4 + 10\, e^{-C_8/T_1} + 6\, e^{-C_7/T_1}}$$

$$\alpha_{3,0} = \alpha_{2,0}$$

$$\alpha_{1,1} = \begin{pmatrix} 1 \\ 1 - \varphi_1 \end{pmatrix} \tilde{b}$$

$$\alpha_{2,1} = \begin{pmatrix} 1 \\ 1 - \varphi_1 \end{pmatrix}$$

$$\alpha_{3,1} = (1 + 1.24\, e^{C_9/T_1})\, \alpha_{2,1}$$

SECOND ORDER

$$T_2 = T_{2,0} + 0.49 \frac{g_2}{g_1} + \frac{\rho_1}{1.72}$$

$$T_{2,0} = 0.49 \left(1 - \frac{f_1^2}{g_1}\right) - \frac{1}{1.72}$$

$$\beta_2 = \beta_{2,0} + \beta_{2,1}\, g_2 + \beta_{2,2}\, \rho_1$$

$$\beta_{2,0} = \frac{\frac{3}{2} - \sqrt{\lambda}\eta + \left(1 + \frac{A\theta_d}{T_2}\right) T_{2,0}}{2(1 + C_2 T_1\, e^{-\theta_d/T_1})}$$

$$\beta_{2,1} = \frac{0.49\ (1 + \frac{A\Theta_d}{T_2})}{2g_1\ (1 + C_2 T_1\ e^{-\theta_d/T_1})}$$

$$\beta_{2,2} = 1.184\ g_1\ \beta_{2,1}$$

$$\varphi_2 = \varphi_{2,0} + \varphi_{2,1}\ g_2 + \varphi_{2,2}\ \rho_1$$

$$\varphi_{2,0} = \frac{\frac{3}{2} - \sqrt{\lambda\eta} + 2.5\ T_{2,0}\ (1 + \frac{A\Theta_i}{2.5\ T_2})}{2[1 + T_1^{2.5}\ C_3\ e^{-\theta_i/T_1}]}$$

$$\varphi_{2,1} = \frac{1.225\ (1 + \frac{A\Theta_i}{2.5\ T_2})}{2g_1\ [1 + T_1^{2.5}\ C_3\ e^{-\theta_i/T_1}]}$$

$$\varphi_{2,2} = 1.184\ \varphi_{2,1}\ g_1$$

$$B_{1,2} = \begin{pmatrix} 1 \\ 1 - \varphi_1 \end{pmatrix} T_2 \left[(1 + \frac{Ac_4}{T_2})\ \tilde{b} + C_5 T_1 + 3C_6 T_1^3\right] + \begin{pmatrix} \beta_2 \\ -\varphi_1\varphi_2 \end{pmatrix} \tilde{b}$$

$$B_{2,2} = 2T_2 \left\{(1 + \frac{Aa}{T_2})\ T_1 f(a) - (1 + \frac{Ab}{T_2}) T_1 f(b) + T_1\left[f(aT_1) - f(bT_1)\right]\right\}$$

$$B_{3,2} = 2T_2\left[\frac{B_{3,1}}{2}\ (1 + \frac{Ab}{T_2}) + T_1 f(bT_1)\right]$$

$$\alpha_{1,2} = \begin{pmatrix} 1 \\ 1 - \varphi_1 \end{pmatrix} T_2 \left\{\frac{Ac_4}{T_2}\ \tilde{b} + C_5 T_1 + 3C_6 T_1^3 - 2\tilde{b}\left[\frac{\pi^4 T_1^3}{5} - \frac{Aa}{T_2}\ f(a) - f(aT_1)\right] \Big/ \left[\frac{2\pi^4 T_1^3}{15}\right.\right.$$

$$\left.\left. - 2f(a)\right]\right\} + \begin{pmatrix} \beta_2 \\ -\varphi_1\varphi_2 \end{pmatrix} \tilde{b}$$

$$\alpha_{2,2} = \begin{pmatrix} \beta_2 \\ -\varphi_1\varphi_2 \end{pmatrix} + \begin{pmatrix} 1 \\ 1 - \varphi_1 \end{pmatrix} \left[AC_7 - \left(\frac{10\, Ac_8 e^{-C_8/T_1} + 6Ac_7 e^{-C_7/T_1}}{4 + 10e^{-C_8/T_1} + 6e^{-C_7/T_1}} \right) \right]$$

$$\alpha_{3,2} = (1 + 1.24\, e^{C_9/T_1})\, \alpha_{2,2} - 1.24\, Ac_9 \alpha_{2,1}\, e^{C_9/T_1}$$

THIRD ORDER COEFFICIENTS

$$T_3 = 0.49\, (2u_1 + \frac{g_3 - 2u_1 f_1 f_2}{g_1}) - 0.039\, (1 + \frac{g_2 - f_1^2}{g_1})^2 - \frac{2u_1}{1.72} - 0.36\, T_2^2$$

$$\beta_3 = \Big[A\theta_d (T_2 + 1.5 - \sqrt{\lambda\eta} + \tfrac{1}{2} A\theta_d) + C\theta_d + T_3 + 2u_1$$

$$- (\sqrt{\lambda\eta} - \tfrac{1}{2})(k_1 + u_1 + r_1) + (\tfrac{3}{2} - \sqrt{\lambda\eta})^2 + T_2(\tfrac{3}{2} - \sqrt{\lambda\eta}) \Big] /$$

$$\Big[2(1 + C_2 T_1 e^{-\theta_d/T_1}) \Big] - 2\beta_2^2 (C_2 T_1 e^{-\theta_d/T_1} + \tfrac{1}{4})$$

$$\varphi_3 = \Big[\tfrac{5}{2} T_3 + \tfrac{15}{8} T_2^2 + 2u_1 - (\sqrt{\lambda\eta} - \tfrac{1}{2})(k_1 + u_1 + r_1) + \tfrac{5}{2} T_2 (\tfrac{3}{2} - \sqrt{\lambda\eta})$$

$$+ B\theta_i + C\theta_i + (\tfrac{3}{2} - \sqrt{\lambda\eta})^2 + A\theta_i (\tfrac{5}{2} T_2 + \tfrac{3}{2} - \sqrt{\lambda\eta}) \Big] /$$

$$\Big[2(1 + C_3 T_1^{5/2} e^{-\theta_i/T_1}) \Big] - 2\varphi_2^2 (C_3 T_1 e^{-\theta_i/T_1} + \tfrac{1}{4})$$

$$\alpha_1' = \frac{T_2 \Big[\frac{2\pi^4 T_1^3}{5} - \frac{2Aa}{T_2} f(a) - 2f(aT_1) \Big]}{\frac{2\pi^4 T_1^3}{15} - 2f(a)}$$

$$\alpha_2' = \left\{ \frac{2\pi^4 T_1^3}{5} \quad (T_3+T_2^2) - 2f(a)(Ba+Ca) - AaT_2 f(aT_1) \right.$$

$$\left. - 2e^{-a/T_1} \left[3a^2 T_1 T_3 + 6aT_1^2(2T_3+T_2^2) + 18T_1^3(T_3+T_2^2) \right] \right\} /$$

$$\left[\frac{2\pi^4 T_1^3}{15} - 2f(a) \right]$$

$$\alpha_3' = \left[10Ac_8 e^{-C_8/T_1} + 6Ac_7 e^{-C_7/T_1} \right] / \left[4+10^{-C_8/T_1} + 6e^{-C_7/T_1} \right]$$

$$\alpha_4' = \left[10(Bc_8+Cc_8)e^{-C_8/T_1} + 6(Bc_7+Cc_7)e^{-C_7/T_1} \right] /$$

$$\left[4+10e^{-C_8/T_1} + 6e^{-C_7/T_1} \right]$$

$$\alpha_{1,3} = \begin{pmatrix} \beta_3 \\ -\varphi_1\varphi_3 \end{pmatrix} \tilde{b} + \begin{pmatrix} \beta_2 \\ -\varphi_1\varphi_2 \end{pmatrix} \left[\frac{\alpha_{1,2} - \begin{pmatrix} \beta_2 \\ -\varphi_1\varphi_2 \end{pmatrix} \tilde{b}}{\begin{pmatrix} 1 \\ 1-\varphi_1 \end{pmatrix}} \right]$$

$$+ \begin{pmatrix} 1 \\ 1-\varphi_1 \end{pmatrix} \left\{ C_5 T_1 T_3 + 3C_6 T_1^3 (T_3+T_2^2) + \tilde{b}\ (Bc_4+Cc_4) \right.$$

$$+ Ac_4 (C_5 T_1 T_2 + 3C_6 T_1^3 T_2) - \alpha_1' T_2 \left(\frac{Ac_4}{T_4} \tilde{b} + C_5 T_1 \right.$$

$$\left. \left. + 3C_6 T_1^3 \right) - \tilde{b}\ (\alpha_2' - \alpha_1'^2) \right\}$$

$$\alpha_{2,3} = \begin{pmatrix} \beta_3 \\ -\varphi_1\varphi_3 \end{pmatrix} + \begin{pmatrix} \beta_2 \\ -\varphi_1\varphi_2 \end{pmatrix}\left[\frac{\alpha_{2,2} - \begin{pmatrix} \beta_2 \\ -\varphi_1\varphi_2 \end{pmatrix}}{\begin{pmatrix} 1 \\ 1-\varphi_1 \end{pmatrix}}\right]$$

$$+ \begin{pmatrix} 1 \\ 1-\varphi_1 \end{pmatrix}\left[Bc_7 + Cc_7 - Ac_7\alpha_3' - (\alpha_4' - \alpha_3'^2)\right]$$

$$\alpha_{3,3} = (1+1.24e^{C_9/T_1})\,\alpha_{2,3} + 1.24e^{C_9/T_1}\left[\alpha_{2,1}(Bc_9 - Cc_9) - \alpha_{2,2}AC_9\right]$$

$$B_{1,3} = \begin{pmatrix} \beta_3 \\ -\varphi_1\varphi_3 \end{pmatrix}\tilde{b} + \begin{pmatrix} \beta_2 \\ -\varphi_1\varphi_2 \end{pmatrix} T_2\left[\left(1 + \frac{Ac_4}{T_2}\right)\tilde{b} + C_5T_1 + 3C_6T_1^3\right]$$

$$+ \begin{pmatrix} 1 \\ 1-\varphi_1 \end{pmatrix}\left[(T_3 + Cc_4 + Bc_4 + Ac_4T_2)\,\tilde{b} + C_5T_1T_3\right.$$

$$\left. + 3C_6T_1^3(T_3+T_2^2) + (C_5T_1 + 3C_6T_1^3)\,T_2^2\left(1 + \frac{Cc_4}{T_2}\right)\right]$$

$$B_{2,3} = 2T_1f(a)\,(T_3 + Ba + Ca + AaT_2) + 2T_1e^{-a/T_1}\left[T_2^2\left(1 + \frac{Aa}{T_2}\right)\right.$$

$$(3a^2T_1 + 12aT_1^2 + 18T_1^3) + 3a^2T_1T_3 + 6aT_1^2\,(2T_3 + T_2^2)$$

$$\left. + 18T_1^3\,(T_3 + T_2^2)\right] - B_{3,3}$$

$$B_{3,3} = 2T_1f(b)\,(T_3 + Bb + Cb + AbT_2) + 2T_1e^{-b/T_1}\left[T_2^2\,(1 + \frac{Ab}{T_2})\right.$$

$$\left.(3b^2T_1 + 12bT_1^2 + 18T_1^3) + 3b^2T_1T_3 + 6bT_1^2(2T_3+T_2^2) + 18T_1^3(T_3+T_2^2)\right]$$

$$F_1 = \Gamma_1\alpha_{1,1}(\alpha_{1,0}A_{1,1}-4\pi B_{1,0}) + \Gamma_2\alpha_{2,0}\left[\alpha_{2,1}(A_{2,1}-4\pi B_{2,1})+\alpha_{3,1}(A_{3,1} - 4\pi B_{3,1})\right]$$

$$F_2 = \Gamma_1\left[\alpha_{1,0}(\alpha_{1,1}A_{1,2} + \alpha_{1,2}A_{1,1} - 4\pi B_{1,0}B_{1,2}\right] + \Gamma_2\alpha_{2,0}$$
$$\left[\alpha_{2,1}(A_{2,2}-4\pi B_{2,2}) + \alpha_{2,2}(A_{2,1}-4\pi B_{2,1}) + \alpha_{3,1}(A_{3,2} - 4\pi B_{3,2}) + \alpha_{3,2}(A_{3,1}-4\pi B_{3,1})\right]$$

$$F_3 = \Gamma_1\left[\alpha_{1,0}(\alpha_{1,1}A_{1,3} + \alpha_{1,2}A_{1,2} + \alpha_{1,3}A_{1,1}) - 4\pi B_{1,0}B_{1,3}\right]$$
$$+ \Gamma_2\alpha_{2,0}\left[\alpha_{2,1}(A_{2,3} - 4\pi B_{2,3}) + \alpha_{2,2}(A_{2,2}-4\pi B_{2,2})\right.$$
$$+ \alpha_{2,3}(A_{2,1}-4\pi B_{2,1}) + \alpha_{3,1}(A_{3,3}-4\pi B_{3,3})$$
$$\left.+ \alpha_{3,2}(A_{3,2}-4\pi B_{3,2}) + \alpha_{3,3}(A_{3,1}-4\pi B_{3,1})\right]$$

$$H_1 = 2\sqrt{\lambda}\eta(r_1-u_1-k_1) + 2(k_1 + 4r_1 + 5u_1)$$

$$H_2 = 9r_2 + 6u_1^2 + 15u_2 + 3k_2 + 7r_1^2 + 23r_1u_1 + 7r_1k_1$$
$$+ 3k_1u_1+4\sqrt{\lambda}\eta\left[r_2 + r_1^2 - k_2 - u_2 - k_1u_1 - r_1(u_1 + k_1)\right]$$

$$\sigma_1 = \frac{1}{2} - \sqrt{\lambda}\eta + 0.84\ (1 + \frac{g_2 - f_1^2}{f_1})$$

$$\sigma_2 = 0.84\ (2u_1 + \frac{g_2 - f_1^2}{g_1} + \frac{g_3 - 2u_1 f_1 f_2}{g_1} + 1) - (\sqrt{\lambda}\eta - \frac{1}{2})(k_1 + u_1 + r_1)$$

$$-(\frac{3}{2} - \sqrt{\lambda}\eta)(\sqrt{\lambda}\eta - \frac{1}{2}) - 0.067\ (1 + \frac{g_2 - f_1^2}{g_1})^2 + 0.84(\frac{1}{2} - \sqrt{\lambda}\,\eta)(1 + \frac{g_2 - f_1^2}{g_1})$$

$$\sigma_3 = f_1\ \{[(2r_2 + r_1^2) f_1 + 6 r_1 u_1 f_2] - 2\eta[3(2r_2 + r_1^2)\ \frac{df_1}{d\eta}$$

$$+ 4 r_1 u_1\ \frac{df_2}{d\eta}]\} + u_1 f_2[3u_1 f_2 + 2 f_1 r_1 - 2\eta(4 r_1\ \frac{df_1}{d\eta} + u_1\ \frac{df_2}{d\eta})]$$

$$\sigma_4 = -\ 4 r_1 g_2 f_1 + 2\eta f_1[4 r_1\ \frac{dg_2}{d\eta} + (2r_2 + r_1^2)\ 3\ \frac{dg_1}{d\eta}]$$

$$-\ 2u_1 f_2 g_2 + 2\eta u_1 f_2 (4 r_1\ \frac{dg_1}{d\eta} + \frac{dg_2}{d\eta})$$

Appendix II

ERROR ESTIMATION FOR THE QUASI-ONE-DIMENSIONAL APPROXIMATION

In this appendix we will show that within the framework of differential approximation, the quasi-one-dimensional approximation that leads to Eq. (5b) introduces an error of the order ϵ^2, which is small.

Equation (5a) can be written in body oriented coordinates as follows:

$$\frac{1}{r}\left[\frac{\partial r(q_x)_\nu}{\partial x} + \frac{\partial r\tilde{k}(q_y)_\nu}{\partial y}\right] = -\alpha_\nu\,[(I_o)_\nu - 4\pi B_\nu] \tag{A-1}$$

For a thin shock layer, one may approximate $\tilde{k} \simeq 1$, $r \approx r_s$. Thus Eq. (A-1) becomes

$$\frac{1}{r_s}\frac{\partial r_s(q_x)_\nu}{\partial x} + \frac{\partial (q_y)_\nu}{\partial y} = -\alpha_\nu\,[(I_o)_\nu - 4\pi B_\nu] \tag{A-2}$$

After frequency integration and transforming x and y to ξ and η, we find

$$\frac{\epsilon\rho_s\mu_s}{\rho}\frac{\partial r_s(q_x)_i}{\partial \xi} - \left(v + 2\eta\frac{dr_s}{d\xi}\frac{\epsilon\rho_s\mu_s}{\rho}\right)\frac{\partial (q_x)_i}{\partial \eta} + u\frac{\partial (q_y)_i}{\partial \eta} = -\lambda_i r_s\,[(\alpha I_o)_i - 4\pi B_i] \tag{A-3}$$

Equation (7) is now needed for the determination of q_x. After frequency integration and transformation into ξ and η variables, Eq. (7) becomes

$$\frac{\epsilon\rho_s\mu_s r_s}{\rho}\frac{\partial (I_o)_i}{d\xi} - \left(v + 2\eta\frac{dr_s}{d\xi}\frac{\epsilon\rho_s\mu_s}{\rho}\right)\frac{\partial (I_o)_i}{\partial \eta} = -3\lambda_i r_s(\alpha q_x)_i \tag{A-4}$$

Similar to the series given by Eqs. (44) and (45), we write

$$(q_x)_i = q_{i,1}(\eta)\,\xi + q_{i,2}(\eta)\,\xi^3 + q_{i,3}(\eta)\,\xi^5 + \ldots \qquad \text{(A-5)}$$

and from Eqs. (82) and (84),

$$V = \epsilon g_1^{0.84}(-2\bar{\eta} + v_2(\eta)\,\xi^2 + v_3(\eta)\,\xi^4 + \ldots) \qquad \text{(A-6)}$$

$$\frac{\rho_s \mu_s}{\rho} = g_1^{0.84}\left[1 + (\sigma_1-\rho_1-\mu_1)\,\xi^2 + (\sigma_2-\mu_2-\rho_2+\rho_1\mu_1 - \sigma_1\mu_1 - \sigma_1\rho_1)\xi^4+\ldots\right] \qquad \text{(A-7)}$$

Substituting Eqs. (A-5) to (A-7) and Eqs. (44) and (45) into Eqs. (A-3) and (A-4), collecting terms of the same order in ξ, we obtain

$$f_1 \frac{\partial Q_{i,1}}{\partial \eta} + 2\epsilon g_1^{0.84}\, q_{i,1} = -\lambda_i(\alpha_{i,o}\alpha_{i,1}A_{i,1} - 4\pi\, B_{i,o}B_{i,1}) \qquad \text{(A-8)}$$

$$\epsilon g_1^{0.84}\left\{2A_{i,2} - \left[v_2 - 2\eta(3r_1+\sigma_1-\mu_1-\rho_1)\right]\frac{\partial A_{i,1}}{\partial \eta}\right\} = -3\lambda_i\alpha_{i,o}\alpha_{i,1}q_{i,1} \qquad \text{(A-9)}$$

$$f_1 \frac{dA_{i,1}}{d\eta} = -3\lambda_i\,\alpha_{i,o}\alpha_{i,1}Q_{i,1} \qquad (55)$$

$$f_1 \frac{dA_{i,2}}{d\eta} = 3u_1 \left(\frac{f_2}{f_1}\right) \lambda_i \alpha_{i,o} \alpha_{i,1} Q_{i,1} - 3\lambda_i \alpha_{i,o} \left[\alpha_{i,1} Q_{i,2} + (r_1 \alpha_{i,1} + \alpha_{i,2}) Q_{i,1}\right] \quad (60)$$

From the above equations, it is seen that if we assume $Q_{i,1}$, $Q_{i,2}$ to be of order unity, and since $\alpha_{i,1}$, $\alpha_{i,2}$ are of the same order of magnitude, from Eq. (60) $A_{i,2}$ is of order $(\lambda_i \alpha_{i,o} \alpha_{i,1})$ (note that $f_1 \frac{d}{d\eta} = \frac{d}{d\omega}$, $d\omega$ is $O(1)$ across the shock layer).

In view of Eq. (56), we conclude from Eq. (A-9) that $q_{i,1}$ is of order ϵ. From Eq. (A-8) it can be seen that the term omitted in the approximation of Eq. (56) is of order ϵ^2. The resulting simplification of the radiant flux divergence is thus valid for thin radiating shock layer models.

Appendix III

SERIES EXPANSION OF LARGE PARAMETER EXPONENTIAL FUNCTION

A strong exponential temperature dependence is experienced by the absorption coefficient of air. For the three band model, this temperature dependence is indicated by the analytical expressions for the absorption and emission coefficients (Eqs. 34-39). Description of temperature as a series expansion about the body (Eq. 46) requires an approximation to the exponential function

$$e^{-C/T} = e^{-C/T_1[1-T_2\xi^2-(T_3-T_2^2)\xi^4+\ldots} \tag{A-10}$$

found in the absorption and emission coefficients. The typical Taylor series expansion of this exponential is given by

$$e^{-C/T} = e^{-C/T_1}\left[1 + \frac{C}{T_1}T^2\xi^2 + \left(\frac{1}{2}\left(\frac{CT_2}{T_1}\right)^2 + (T_3-T_2^2)\frac{C}{T_1}\right)\xi^4 + \ldots\right. \tag{A-11}$$

Because of the strong exponential temperature dependence of the absorption coefficient in air, the value of C is of order 10. The resulting large factors CT_2/T_1 and $(T_3-T_2^2)\,C/T_1$ restrict the region of convergence of the Taylor series expansion to small values of ξ as shown by F_2 in Fig. A-1. In order to obtain an approximate description of this exponential function at greater distances from the stagnation point than 15°, ($x = .2$), additional terms must be used in the Taylor series expansion or another form of a series expansion must be used. Because of the inherent complexity of higher order series solutions, the latter course was selected.

A general three term series expansion of an exponential function is assumed

$$e^{+SX^n} = 1 + AX^n + BX^{2n} \tag{A-12}$$

where the constants A and B are determined from boundary conditions on the exponential at any value X. In contrast to the Taylor series expansion where $x = 0$ is utilized, an arbitrary value $X = X_o$ is selected such that the Eq. (A-12) represents an approximate description of the exponential to large value of X ($\sim .85$ or 50^o). Consequently, the constants A and B can be defined

$$B = \frac{1}{X_o^{2n}}\left[1 - e^{SX_o^n}(X_o^n S - 1)\right]$$
$$A = S\, e^{SX_o^n} - 2BX_o^n \tag{A-13}$$

For a three term series, the coefficients of Eq. (A-13) insure a positive value to the exponential function at all values of X. This is essential to the physics of the absorption mechanism.

If Eq. (A-10) were written as

$$e^{-C/T}/e^{-C/T_1} = e^{CT_2/T_1\,\xi^2}\, e^{C(T_3-T_2^2)/T_1\,\xi^4} \tag{A-14}$$

and the second and third exponentials approximated by a series similar to Eq. (A-12), the resulting approximation, F_3, is plotted in Fig. A-1 (the series to second order is noted as $F_3(2)$ and to third order, $F_3(3)$). As would be anticipated, F_3 is not as accurate as the Taylor series at small values of

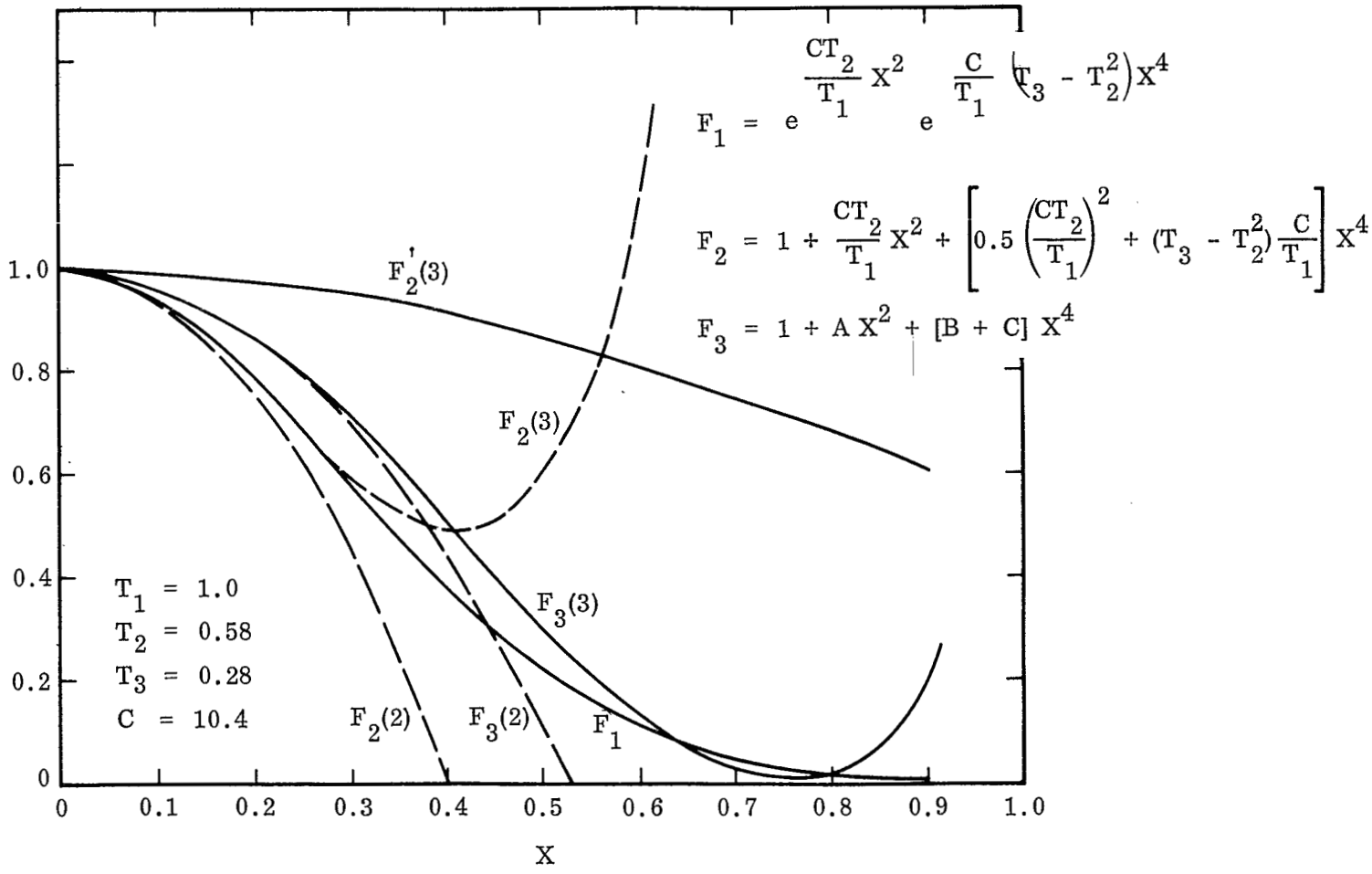

Fig. A-1 Comparison of Series Approximations to a Large Parameter Exponential Function

X; however, it represents the exponential function at higher X values with three terms. In comparison results where the Taylor series were utilized (small values of X), the influence of the approximate series was shown to have a negligible effect upon the coupling investigation.

In this investigation the constants A and B were determined by the numerical code for each value of C, T_1, T_2 and T_3. A value of $X_o = .75$ was used.

Appendix IV

POWER SERIES COEFFICIENTS

In this appendix, the coefficients u_1 , r_1 , k_1 , ρ_1 , etc. in the series represented by Eqs. (44) will be determined for a conical shape body. A relationship between the distance along a body ξ and the body angle, θ , will also be obtained.

We first determine the coefficients. For a body oriented coordinate system, a description of an oblique shock is given by (see Fig. 1):

$$
\begin{aligned}
u_s &= \operatorname{Sin}\varphi \operatorname{Cos}\delta + \epsilon \operatorname{Cos}\varphi \operatorname{Sin}\delta \\
p_s &= (1-\epsilon)\operatorname{Cos}^2\varphi \\
\rho_s &= \frac{(\gamma+1)\, M_\infty^{\,2} \operatorname{Cos}^2\varphi}{(\gamma-1)\, M_\infty^{\,2} \operatorname{Cos}^2\varphi + 2} \qquad \text{(A-15)} \\
k_s &= -\frac{d\sigma}{d\xi_s} \\
r_s &= \int_0 \operatorname{Sin}\sigma\, d\xi_s
\end{aligned}
$$

where $\varphi = f(\xi_s)$ is the shock angle,

$$\delta = \theta - \varphi$$

and $$\sigma = \frac{\pi}{4} - \varphi \ .$$

Lomas and Inoye (Ref. 10) has shown that for the inviscid, adiabatic hypersonic case, the conical shock model is a valid assumption for a conical body when the free stream Mach number is greater than 5 and γ ranges from 1.1 to 1.667. In our study, we will therefore assume the shock shape to be conical. The conical shock (in dimensionless form) can be described by the equation

$$\frac{r^2}{2\bar{X}} + \frac{1}{2} B_s \bar{X} = 1 \tag{A-16}$$

where $\bar{X}$ is the distance from the shock stagnation point along the line of symmetry, r is vertical distance from line of symmetry and B_s is the shock bluntness parameter. From Eq. (A-16), we obtain

$$\text{Cot } \varphi = \frac{dr}{d\bar{X}} = \frac{1-B_s\bar{X}}{\sqrt{2\bar{X}-B_s\bar{X}^2}} \tag{A-17}$$

$$\frac{d\xi_s}{d\bar{X}} = \sqrt{1 - B_s + \frac{1}{2\bar{X} - \bar{X}^2 B_s}} \tag{A-18}$$

One then can find the derivatives of φ with respect to ξ_s . Similarly the nondimensional equation for a conical body is

$$\frac{r^2}{2\bar{X}_\theta} + \frac{1}{2} B_b \bar{X}_\theta = \frac{R_b}{R_s} \tag{A-19}$$

Consequently where $\bar{X}_\theta$ is distance along the line of symmetry from body stagnation point.

Consequently,

$$\text{Cot}\,\theta = \frac{dr}{d\bar{X}_\theta} = \frac{\left(\frac{R_b}{R_s}\right) - B_b\,\bar{X}_\theta}{\sqrt{2\left(\frac{R_b}{R_s}\right)\bar{X}_\theta - B_b\bar{X}_\theta^{\,2}}} \tag{A-20}$$

$$\frac{d\xi}{d\bar{X}} = \sqrt{1 - B_b + \frac{\left(\frac{R_b}{R_s}\right)^2}{2\left(\frac{R_b}{R_s}\right)\bar{X}_\theta - B_b\bar{X}_\theta^{\,2}}} \tag{A-21}$$

where the body radius R_b has been normalized by the shock radius R_s .

From Eqs. (A-20) and (A-21), one can find the derivatives of θ with respect to ξ .

As noted in the text, the calculational procedure was to assume a shock shape, (i.e. gives B_s) calculate the resulting flow field and then iterate on a new shock shape. For an assumed shock shape, the coefficients of the series

$$\xi_s = u_o\xi + \frac{C_1}{3!}\,\xi^3 + \frac{C_2}{5!}\,\xi^5 + \ldots . \tag{A-22}$$

can be found, under the assumption of thin shock layer. The factor u_o can be taken as unity.

The velocity behind the shock u_s , can now be expanded in a Taylor series

$$u_s = (u_s)_o + \left(\frac{du_s}{d\xi}\right)_o \xi + \frac{1}{2}\left(\frac{d^2u_s}{d\xi^2}\right)_o \xi^2 + \frac{1}{3!}\left(\frac{d^3u_s}{d\xi^3}\right) \xi^3 \ldots . \qquad \text{(A-23)}$$

Using Eqs. (A-15) - (A-22), one can evaluate the derivatives $\frac{d^n u_s}{d\xi^n}$ of Eq. (A-23). The Taylor series expansion of u_s can therefore be written

$$u_s = \xi + u_1\xi^3 + u_3\xi^5 + \ldots . \qquad \text{(A-24)}$$

where

$$u_1 = -\frac{1}{6}\{1 + 3(1-B_s) - C_1\} + O(\epsilon)$$

$$u_2 = \frac{1}{5!}\{1 + 3(1-B_s)(29 - 15B_s) - 21\,C_1(1-B_s) - 10\,C_1 + C_2\} + O(\epsilon)$$

Similarly, if the other post shock variables are expanded, we obtain the following expressions for their coefficients (See Eq. 44):

$$\begin{aligned}
r_1 &= -\frac{1}{6} \\
r_2 &= \frac{1}{5!}[1 + 12(1-B_s) - 4C_1] \\
k_1 &= -\frac{3}{2}(1-B_s) \\
k_2 &= \frac{1}{8}(1-B_s)(19 - 15B_s - 4C_1) \\
p_1 &= 1 \\
p_2 &= -\frac{1}{3}[1 + 3(1 - B_s) - C_1] \\
\rho_1 &= \frac{2}{(\gamma-1)\,M_\infty 2 + 2}
\end{aligned} \qquad \text{(A-25)}$$

$$\rho_2 = \frac{(\gamma-1)M_\infty^2}{2+(\gamma-1)M_\infty^2} - \frac{2}{3}\left[1+3(1-B_s) - C_1\right] - \frac{1}{2}\left[\frac{(\gamma-1)M_\infty^2}{(\gamma-1)M_\infty^2+2}\right]^2$$

The relation between ξ and θ is given by Eqs. (A-20) and (A-21).

In the special cases of $B_b = 0$ (paraboloid) and $B_b = 1$ (spherical), Eq. (A-21) can be integrated to yield:

Paraboloid:

$$\cot\theta = \frac{1}{2\bar{X}'} \tag{A-26}$$

$$\xi = a_o \Big/ \left\{2\left[\sqrt{2\bar{X}'(1+2\bar{X}')} + \ell n\left(\sqrt{2\bar{X}'} + \sqrt{1+2\bar{X}'}\right)\right]\right\}$$

Where $\bar{X}' = \bar{X}/a_o$, $a_o = \frac{R_b}{R_s}$

Sphere:

$$\xi = a_o\theta \ . \tag{A-27}$$

NASA-Langley, 1970 —— 33